frontiers in Physiology

ORIGINAL RESEARCH
published: 05 June 2019
doi: 10.3389/fphys.2019.00700

Mutations in $Na_V1.5$ Reveal Calcium-Calmodulin Regulation of Sodium Channel

Eyal Nof[1,2], Leonid Vysochek[1], Eshcar Meisel[1,2], Elena Burashnikov[3], Charles Antzelevitch[3,4,5], Jerome Clatot[3], Roy Beinart[1,2], David Luria[1†], Michael Glikson[1,2†] and Shimrit Oz[1]*

[1] Heart Center, Sheba Medical Center, Ramat Gan, Israel, [2] Sackler School of Medicine, Tel Aviv University, Tel Aviv, Israel, [3] Lankenau Institute for Medical Research, Wynnewood, PA, United States, [4] Lankenau Heart Institute, Wynnewood, PA, United States, [5] Sidney Kimmel Medical College, Thomas Jefferson University, Philadelphia, PA, United States

OPEN ACCESS

Edited by:
Ademuyiwa S. Aromolaran,
SUNY Downstate Medical Center,
United States

Reviewed by:
Brian P. Delisle,
University of Kentucky, United States
Marina Cerrone,
New York University, United States
Carol Ann Remme,
University of Amsterdam, Netherlands

***Correspondence:**
Shimrit Oz
shimrit.oz@sheba.health.gov.il;
shimrit.oz.fr@gmail.com

†Present address:
David Luria,
Hadassah Medical Center, Jerusalem, Israel
Michael Glikson,
Shaare Zedek Medical Center, Jerusalem, Israel

Specialty section:
This article was submitted to Cardiac Electrophysiology, a section of the journal Frontiers in Physiology

Received: 04 February 2019
Accepted: 20 May 2019
Published: 05 June 2019

Citation:
Nof E, Vysochek L, Meisel E, Burashnikov E, Antzelevitch C, Clatot J, Beinart R, Luria D, Glikson M and Oz S (2019) Mutations in $Na_V1.5$ Reveal Calcium-Calmodulin Regulation of Sodium Channel. Front. Physiol. 10:700. doi: 10.3389/fphys.2019.00700

Mutations in the *SCN5A* gene, encoding the cardiac voltage-gated sodium channel $Na_V1.5$, are associated with inherited cardiac arrhythmia and conduction disease. Ca^{2+}-dependent mechanisms and the involvement of β-subunit ($Na_V\beta$) in $Na_V1.5$ regulation are not fully understood. A patient with severe sinus-bradycardia and cardiac conduction-disease was genetically evaluated and compound heterozygosity in the *SCN5A* gene was found. Mutations were identified in the cytoplasmic DIII-IV linker (K1493del) and the C-terminus (A1924T) of $Na_V1.5$, both are putative CaM-binding domains. These mutants were functionally studied in human embryonic kidney (HEK) cells and HL-1 cells using whole-cell patch clamp technique. Calmodulin (CaM) interaction and cell-surface expression of heterologously expressed $Na_V1.5$ mutants were studied by pull-down and biotinylation assays. The mutation K1493del rendered $Na_V1.5$ non-conductive. $Na_V1.5_{K1493del}$ altered the gating properties of co-expressed functional $Na_V1.5$, in a Ca^{2+} and $Na_V\beta1$-dependent manner. $Na_V1.5_{A1924T}$ impaired $Na_V\beta1$-dependent gating regulation. Ca^{2+}-dependent CaM-interaction with $Na_V1.5$ was blunted in $Na_V1.5_{K1493del}$. Electrical charge substitution at position 1493 did not affect CaM-interaction and channel functionality. Arrhythmia and conduction-disease -associated mutations revealed Ca^{2+}-dependent gating regulation of $Na_V1.5$ channels. Our results highlight the role of $Na_V1.5$ DIII-IV linker in the CaM-binding complex and channel function, and suggest that the Ca^{2+}-sensing machinery of $Na_V1.5$ involves $Na_V\beta1$.

Keywords: β1-subunit, calmodulin, cardiac arrhythmia, channelopathies, DIII-IV linker, heart, *SCN5A*, sodium current

INTRODUCTION

Sodium current (I_{Na}) upstroke is a hallmark of the action-potential in excitable cells. The *SCN5A* gene encodes the pore-forming α-subunit of the cardiac sodium channel $Na_V1.5$. $Na_V1.5$ channels are expressed in cardiomyocytes as well as the cardiac His-Purkinje system. Accordingly, $Na_V1.5$ loss-of-function mutations are associated with cardiac arrhythmia and conduction defects (Schott et al., 1999; Tan et al., 2001; Holst et al., 2010; Zumhagen et al., 2013). Although I_{Na} does not contribute to the action potential of pacemaker cells, its presence in the periphery of the

sinoatrial node can modulate impulse conduction and heart rate (Kodama et al., 1997). Hence, loss-of-function mutations in *SCN5A* can result in a nodal dysfunction (Benson et al., 2003; Lei et al., 2008; Gui et al., 2010; Ziyadeh-Isleem et al., 2014; Chiang et al., 2015; Milanesi et al., 2015).

The $Na_V1.5$ α-subunit is composed of four homologous domains (DI-DIV), each containing six transmembrane repeats. The domains are joined by three cytosolic linkers and flanked by cytosolic C- and N-termini (see **Figure 1C**). The α-subunit forms a functional monomer; however, multi-channel assembly and functional coupling among monomeric channels have been reported (Keller et al., 2005; Poelzing et al., 2006; Clatot et al., 2017). Moreover, the α-subunit is the core of a macromolecular complex that interacts with auxiliary proteins that modulate expression, trafficking, localization and gating of $Na_V1.5$; among them the regulatory β-subunits ($Na_V\beta$) and the Ca^{2+}-sensor calmodulin (CaM) (Abriel, 2010).

$Na_V1.5$ is regulated by Ca^{2+}, but the role and mechanism of this regulation is still debated (Van Petegem et al., 2012; Ben-Johny et al., 2014; Gabelli et al., 2016; Pitt and Lee, 2016; Johnson, 2019). CaM interacts with $Na_V1.5$ C-terminus (CT) (Gabelli et al., 2014; Wang et al., 2014), and the linker between domains DIII-IV (DIII-IV linker) (Sarhan et al., 2012; Johnson et al., 2018). However, the contribution of each CaM-interaction domain to the Ca^{2+}-sensing machinery of $Na_V1.5$ is not fully established. $Na_V\beta1$ interacts non-covalently with $Na_V1.5$ and can modulate I_{Na} gating, as well as transcription and cell-adhesion (Calhoun and Isom, 2014). The involvement of $Na_V\beta1$ in Ca^{2+}-dependent gating regulation is not clear.

We report a novel combination of *SCN5A* variants, K1493del and A1924T, in a patient with sinus-bradycardia and cardiac conduction-disease. Heterozygous A1924T has been previously associated with Brugada syndrome (BrS) (Rook et al., 1999), and homozygous A1924T with sinus-bradycardia with conduction delay (Lopez et al., 2011). Heterozygous K1493del has been associated with isolated conduction disease (Zumhagen et al., 2013). Here, we studied the molecular basis of Ca^{2+}- and CaM-dependent $Na_V1.5$ modulation, using the disease-associated mutations.

MATERIALS AND METHODS

Clinical

The proband and his parents gave written informed consents for both the clinical and genetic studies, which were approved by the Institutional Ethics-Committee of the Sheba Medical Center, Tel-Hashomer (approval 2853/03). Evaluation included resting electrocardiogram (ECG), 24-h Holter monitoring (DELMAR® systems; Impresario 3.04.0089), two-dimensional echocardiography, treadmill exercise test, cardiac MRI, ajmaline test and an electrophysiological-study.

Genetic Analysis

Heparinized blood was drawn from the proband and his parents; DNA was extracted using a commercial kit (Gentra System Inc., Minneapolis, MN, United States) and the exons and exon-intron boundaries of the following genes: *HCN4*, *KCNJ2*, *KCNJ12*, and *SCN5A* were amplified by PCR (Verities PCR, Applied Biosystems, Austin, TX, United States). The PCR products were purified (Exosap-IT, USB, Isogen Life-Science, Netherlands) and sequenced in both directions (BigDye Terminator v3.1 cycle sequencing Kit and 3130xL Genetic Analyzer, Applied Biosystems).

Molecular Biology

A DNA construct of the paternal $Na_V1.5$ variant was prepared with two variants, A1924T and V1251M, on the same DNA construct and denoted as $Na_V1.5_{A1924T*}$. In the maternal channel, $Na_V1.5_{K1493del}$, one lysine of the doublet in positions 1492-3 was deleted. N-terminally tagged green-fluorescent protein (GFP)-$Na_V1.5$ was used (Zimmer et al., 2002). In the constructs K1493A/E/R the second lysine of the lysine-doublet was substituted with the amino-acids indicated. Point-mutations were prepared by site-directed mutagenesis using a standard PCR (Roche, IN, United States), and followed by sequencing of the entire coding sequence. Rat and human -$Na_V\beta1$ ($rNa_V\beta1$ and $hNa_V\beta1$, respectively) were cloned into pcDNA3 vector using HindIII and EcoRI sites, and followed by an internal ribosome entry site (IRES) and the red fluorescent-protein (RFP) sequence between EcoRI and NotI sites ($rNa_V\beta1$/RFP and $hNa_V\beta1$/RFP, respectively). $Na_V1.5$ (NM_198056.2), calmodulin (M19312), $rNa_V\beta1$ (M91808) $hNa_V\beta1$ (NP_001028), and GFP were all in a pcDNA3 vector.

Cell Culture

HEK293 cells were maintained in Dulbecco's Modified Eagle's Medium supplemented with 10% Fetal Bovine Serum, 100 U/ml penicillin, 10 mg/ml streptomycin and 2 mM L-Glutamine (Biological Industries, Kibbutz Beit-Haemek, Israel) at 37°C with 5% CO_2. For electrophysiological experiments, transfections were performed in 35 mm dish using *Trans*-ITx2 (Mirus, Madison, WI, United States) according to the manufacturer's instructions. 1 μg of each construct was used for transfection ($Na_V1.5$, $Na_V\beta1$/RFP, and CaM), except in **Figure 2A**, where 3 μg of GFP tagged- K1493del mutated -$Na_V1.5$ (GFP-$Na_V1.5_{K1493del}$) and $Na_V\beta1$/RFP (μg DNA ratio 1:1) were used. When indicated, 0.5 μg GFP was added as a transfection marker. On the following day, cells were plated on coverslips. For biochemical experiments, cells in 10-cm dishes were transfected using the Calcium-Phosphate method. 5–15 μg DNA of $Na_V1.5$ α-subunit were used, $rNa_V\beta1$ was added in a 0.6 β:α molar ratio unless otherwise indicated. In **Figure 5B**, CaM was added in a 2 CaM:α molar ratio. Experiments were performed 48–72 h after transfection.

HL-1 cells were plated in gelatin/fibronectin-coated dishes, in Claycomb media supplemented with 10% Fetal Bovine Serum, 100 μM norepinephrine (Sigma, St. Louis, Mo, United States), 100 U/ml penicillin, 10 mg/ml streptomycin and 2 mM L-Glutamine (Biological Industries). Transfections using Lipofectamine 3000 (Invitrogen, Carlsbad, CA, United States) were performed in 35 mm dishes. On the following day, cells were plated on gelatin/fibronectin-coated coverslips. Experiments were performed 48 h after transfection.

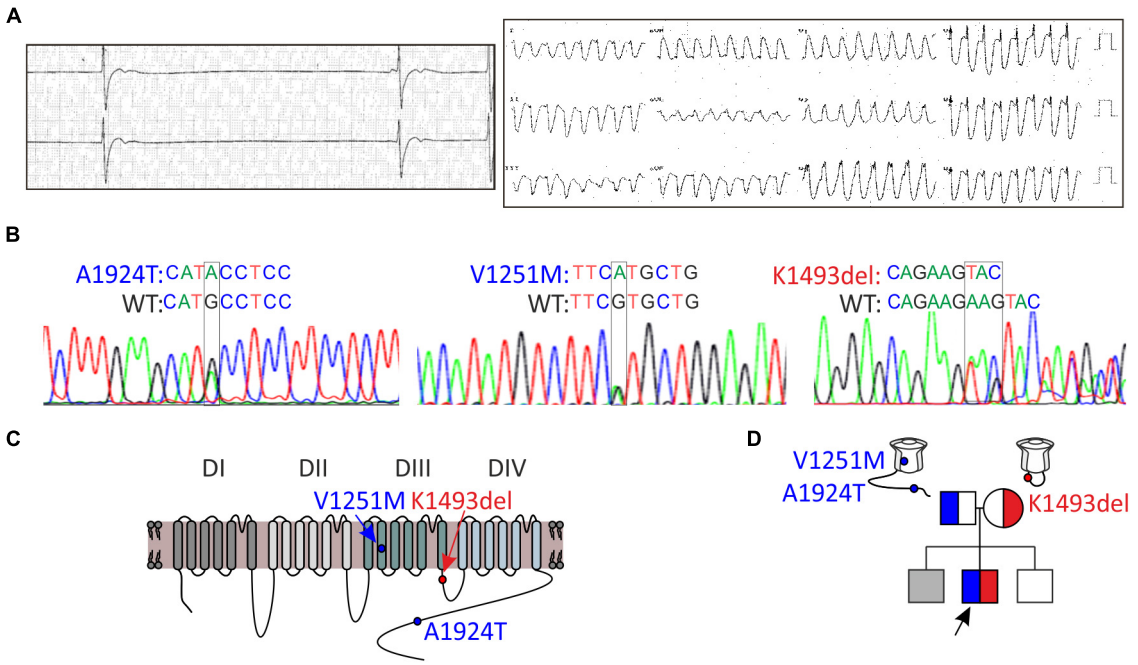

FIGURE 1 | Clinical and genetic characteristics of the proband. **(A)** Left, Holter recording at rest. Right, 12-lead ECG during exercise. **(B)** Sequence chromatogram of *SCN5A* variants. **(C)** Schematic illustration of $Na_V1.5$ protein and the location of the variants found. **(D)** Pedigree tree of the family. Circle indicates female, squares indicate male. The arrow points to the proband. In gray, suspected affected sibling. Red for the maternal allele variant, blue for the paternal allele variant.

RNA Extraction and Quantitative PCR

Total RNA was extracted using RNeasy Plus mini kit (Qiagen, Hilden, Germany). Reverse transcription with random primers was performed using the high capacity cDNA reverse transcription kit (Applied Biosystems, CA, United States). cDNA was amplified using KAPA HiFi HotStart ReadyMix (Roche). Quantitative real-time PCR was performed using ABI Step-one plus sequence detection system (Applied Biosystems) with Fast SYBR Green Master Mix reagent (Applied Biosystems). The primers for mouse genes used were, for $Na_V\beta1$ (NM_011322.2): SCN1B Fw (CGAGGCTGTGTATGGGATGAC)/SCN1B Rv (CCCTCAAAGCGCTCATCTTC), for $Na_V\beta2$ (NM_001014761.2): SCN2B Fw (GTGAACCACAAGCAGT TCTCT)/SCN2B Rv (TGACACGTCGTACTTACTGGG), for $Na_V\beta3$ (NM_001286614.1): SCN3B Fw (TGTAATGTG TCCAGGGAGTTTG)/SCN3B Rv (TTCGGCCTTAGAGACCT TTCTG) and for $Na_V\beta4$ (NM_001013390.3): SCN4B Fw (GGAACCGAGGCAATACTCAGG)/SCN4B Rv (CCGTTAA TAGCGTAGATGGTGGT). Gene expression was quantified using the $2^{\wedge}-\Delta\Delta Ct$ method by normalization to the housekeeping gene GAPDH (Fw: TCGTCCCGTAG ACAAAATGG/Rv: TTGAGGTCAATGAAGGGGTC).

Electrophysiology

Currents were recorded using the whole-cell configuration of the patch-clamp technique at 23°C. Red- and/or green- fluorescent cells were selected for recording. Signals were amplified using an Axopatch 200B patch-clamp amplifier (Axon Instruments, Foster City, CA, United States), sampled at 100 kHz and filtered with a low-pass Bessel filter at 10 kHz. Data was acquired with DigiData1440A and analyzed using pCLAMP 10 software (Axon Instruments). Patch pipettes (Harvard apparatus) resistance was 1.5–4 MΩ. Cells with access resistance over 5 MΩ were discarded. Series resistance was compensated by 85%. Leak currents were subtracted using a P/3 protocol. External solution contained (in mM) 137 NaCl, 4 KCl, 10 Hepes, 10 Glucose, 1.8 $CaCl_2$, and 1 $MgCl_2$ titrated with NaOH to pH 7.4, and adjusted to 310 mOsm. Internal solution contained (in mM) 100 CsF, 25 NaF, 10 Hepes, 10 NaCl, 2 Mg^{2+}-ATP and 10 ethylene glycol-bis (β-aminoethyl ether)-N,N,N′,N′-tetraacetic acid (EGTA), titrated with CsOH to pH 7.2 and adjusted to 295 mOsm, this pipette solution is $(10\ mM\ EGTA)_{in}$. For fast Ca^{2+} chelation, EGTA was replaced with 10 mM 1,2-BIS (2-AMINOPHENOXY)-ETHANE-N,N,N′N′-TETRAACETIC ACID $[(10\ mM\ BAPTA)_{in}]$. For pipette solution with 10 μM Ca^{2+}, EGTA was replaced with 1 mM BAPTA and 1 mM $CaCl_2$ $[(10\ \mu M\ Ca^{2+})_{in}]$. EGTA was replaced with 5 mM N-(2-Hydroxyethyl)ethylenediamine-N,N′,N′-triacetic acid (HEDTA) and 2.5 mM $CaCl_2$ for $[10\ \mu M\ Ca^{2+}]_{in}$/HEDTA (calculated with WebMaxC extended program[1]). Pronase (Roche) was dissolved in $[10\ mM\ EGTA]_{in}$ solution.

Activation protocol was initiated after 2 min, steady-state inactivation (SSI) protocol after 3.25 min and recovery from inactivation after 8 min from the rupture of the cell membrane.

Holding potential was −120 mV. Current-densities were obtained by dividing the peak current by the cell

[1]https://web.stanford.edu/~cpatton/webmaxcE.htm

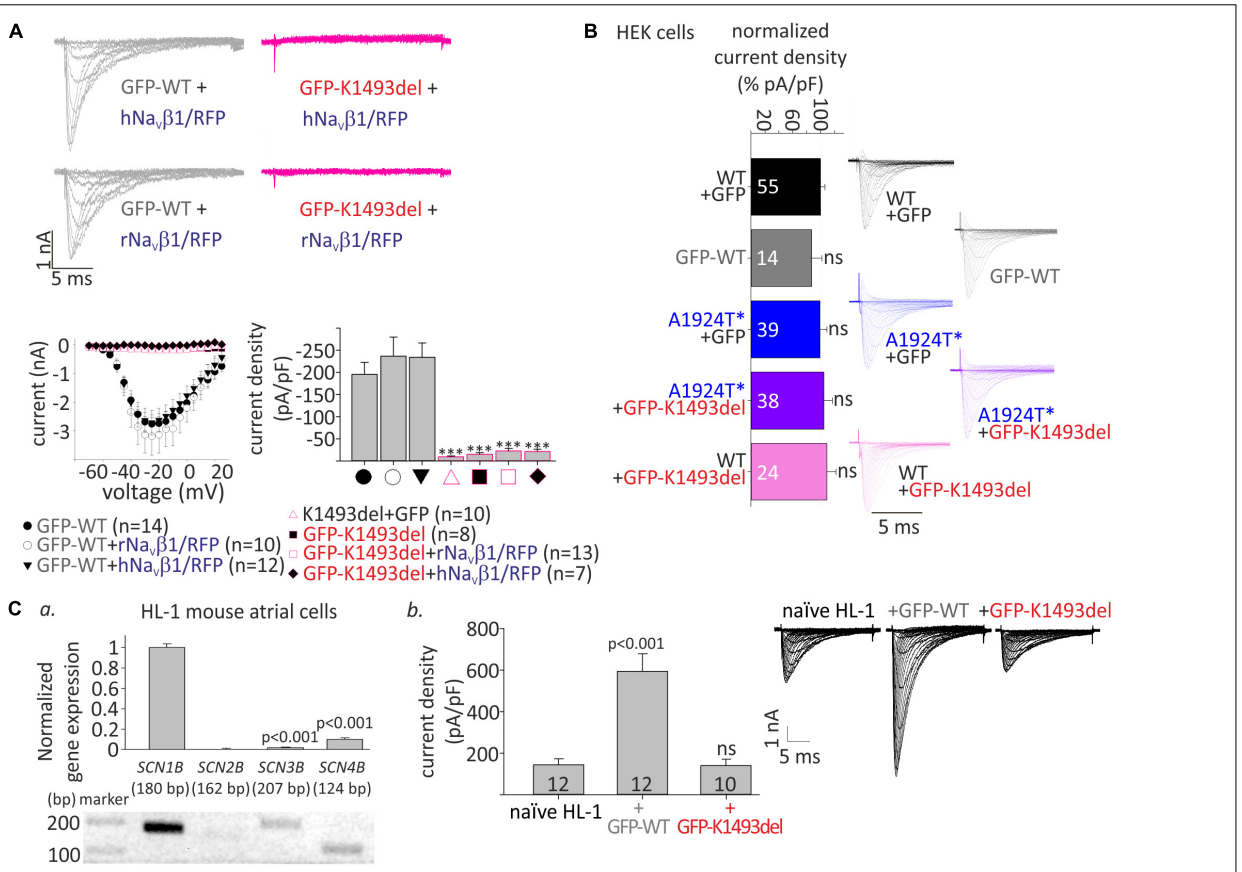

FIGURE 2 | Whole-cell I_{Na} of WT and mutant $Na_V1.5$ in HEK and HL-1 cells. **(A)** Top, representative currents elicited from resting potential by depolarizing steps (–70 until –20 mV in 5 mV interval) in HEK cells. Bottom, voltage-dependent amplitudes and maximal current densities, in cells expressing GFP-$Na_V1.5_{WT}$, GFP-$Na_V1.5_{K1493del}$, and $Na_V1.5_{K1493del}$, with and without r/hNaVβ1 co-expressing RFP in the same vector. All groups were compared to GFP-WT for statistical significance. **(B)** WT and mutant $Na_V1.5$ expressed in HEK cells (without $Na_V\beta$ subunit). Current densities were normalized to the mean current density of $Na_V1.5_{WT}$ in the same experiment and summarized from 9 experiments. Currents in A and the representative currents in B were recorded in $[10\ mM\ EGTA]_{in}$. **(Ca)**, Gene expression levels of *SCNB1-4* in HL-1 cells. Top, gene levels were quantified by real-time PCR and normalized to GAPDH. Bottom, semi-quantitative PCR. **(b)**, I_{Na} measured in naïve and transfected HL-1 cells, in $[10\ mM\ EGTA]_{in}$. Mean current densities and representative cells are shown. Statistical significance was determined by one-way ANOVA, followed by Holm–Sidak test. ns, not significant.

capacitance. Normalized current-densities were calculated by dividing the current density of each cell with the mean $Na_V1.5_{WT}$ current density measured on the same day of the experiment, using the same pipette solution composition. The voltage-dependent activation was calculated by fitting currents, generated by steps from −80 to 40 mV in 5 mV increments for 20 ms, with a modified Boltzmann equation: $I = [Gmax^*(V\text{-}Vrev)]/[1+\exp(Va\text{-}V)/k]$, where I is the peak current for the test potential V, Gmax is maximum conductance, Vrev is the reversal potential, Va is the potential for half-activation or half-availability, and k is the slope factor. The normalized conductance was determined by modified Ohm's law G/Gmax = I/Gmax (V-Vrev).

Steady-state inactivation was assayed by a 20 ms test pulse to −20 mV after a 500 ms pre-pulse to varying voltages (from −140 to −45 mV in 5 mV steps). SSI curves were fitted with Boltzmann equation: $I = 1/[1 + \exp(Va - V)/k]$,

Recovery from inactivation curve was obtained by a 1 s conditioning pulse (I1) to -20 mV followed by a test pulse (I2) to -20 mV after a varying time (1–24 ms, with 1 ms steps) at -120 mV. Fractional recovery was calculated as I2/I1. The time constant (τ) and amplitude (A) of recovery from inactivation were obtained by fitting the data with the function $y = A(1-e^{-t/\tau})$.

Waveform's current decay was fitted to one -exponent fit using Levenberg-Marquardt algorithm, in the form $f(t) = Ae^{-t/\tau} + C$.

Cell Surface Biotinylation and CaM-Beads Pull-Down

For biotinylation experiments, cells were incubated with 0.5 mg/ml EZ-Link Sulfo-NHS-SS-Biotin (Pierce, Rockford, IL, United States) in phosphate buffer saline (pH 8) containing 1 mM Ca^{2+} and 0.5 mM Mg^{2+} (PBS-CM), for 30 min at 4°C. The reaction was terminated by incubation in 50 mM glycine in PBS-CM, for 10 min at 4°C. Cells were scraped and washed with PBS-CM supplemented with 0.5 mM phenylmethylsulfonyl fluoride (PMSF) at 4°C. Cells were lysed in TNE buffer

(in mM): 20 Tris–HCl pH 8, 150 NaCl, 1 EGTA, and 1% NP40 supplemented with 0.5 PMSF, protease inhibitor mixture (Roche), 25 β-glycerol phosphate and 1 Na_3VO_4, for 30 min on ice. A 25 μg sample was taken for input. An equal amount of total protein from each group was incubated with streptavidin-agarose beads (Pierce) for 2 h at 4°C in a rotating device. Samples were washed with TNE buffer supplemented with 0.5 mM PMSF, and proteins were eluted by incubation with sample buffer and freshly added 100 mM DTT, for 1 h at room temperature, and then for 5 min at 65°C. $Na_V1.5_{WT}$ and $Na_V1.5_{K1493del}$ intensities were compared in groups transfected with an equal amount of DNA.

For CaM pull-down experiments, cells were collected in PBS supplemented with 0.5 mM PMSF, and lysed with (in mM) 20 Tris–HCl pH 7.5, 150 NaCl, and 1% Triton x100, supplemented with 0.5 PMSF, protease inhibitor mixture (Roche), 25 β-glycerol phosphate and 1 Na_3VO_4, for 30 min on ice. A 25 μg sample was taken for input. CaM agarose beads (A6112, Sigma) were washed with (in mM) 20 Tris–HCl pH 7.5, 150 NaCl added with either 2 $CaCl_2$, or 10 EGTA, then were incubated with an equal amount of total protein from each group, supplemented with either 2 $CaCl_2$ or 10 EGTA, for 2 h at 4°C in a rotating device. Samples were washed with (in mM) 20 Tris–HCl pH 7.5, 150 NaCl and 1% Triton x100 supplemented with 0.5 PMSF, and proteins were eluted with sample buffer, for 5 min at 65°C.

Normalized $Na_V1.5$ intensity was calculated by dividing $Na_V1.5$ intensity by a normalizer, γ-tubulin for inputs ($Na_V1.5$-$input_{NORM}$ = $Na_V1.5$/γ-tubulin) and Na-K ATPase for plasma membrane-bound fraction ($Na_V1.5$-PM_{NORM} = $Na_V1.5$/Na-K ATPase). Percent of total expression was calculated by dividing intensities of $Na_V1.5$-$input_{NORM}$ with a control group from the same experiment. Trafficking was calculated by dividing $Na_V1.5$-PM_{NORM} by $Na_V1.5$-$input_{NORM}$, and presented as % trafficking from the control group in the same experiment. CaM-beads binding level was quantified by dividing bound by input fractions and normalized to control group in the same experiment.

The antibodies that were used are $hNa_V1.5$ (ASC-013, Alomone, Jerusalem, Israel), Na-K ATPase (ANP-001, Alomone), γ-tubulin (T5192, Sigma), and CaM (05-173, Millipore Corp., Temecula, CA, United States).

Presentation and Statistical Analysis

Densitometry of Western blot bands was analyzed using ImageJ (NIH, United States). Figures were prepared using CorelDrawX8 (Corel Corp., Ottawa, Canada). Statistical analyses were performed using SigmaPlot 13 (Systat Software, CA, United States). Data are presented as mean ± SEM. One-way ANOVA followed by the multiple comparison Holm–Sidak *post hoc* test was used to compare several groups. Two-tailed Student's *t*-test was used to compare two groups.

RESULTS

Clinical and Genetic Data

A 16-year-old male presented with a syncope during exercise. Physical examination revealed a healthy looking young man without any abnormalities. He had bradycardia for many years but was not previously symptomatic. A 24-h Holter recording showed an average heart rate of 50 (range: 24–110) due to sinus-bradycardia and occasional junctional rhythm with sinus-pauses up to 5.8 s (**Figure 1A**, left). A wide complex tachycardia (WCT) of 193 beat-per-minute was recorded during exercise testing (**Figure 1A**, right). Echocardiography and cardiac-MRI did not reveal any structural abnormalities or areas of late gadolinium enhancement. Ajmaline provocation test ruled out BrS. Electrophysiological-study demonstrated a prolonged A-H interval of 260 ms and H–V interval of 75 ms. During rapid pacing (420 CL), the H–V interval increased to over 100 ms. Atrial-flutter was inducible with 1:1 conduction, leading to "clinical" WCT. The proband developed symptomatic bradycardia and a permanent pacemaker was eventually implanted.

DNA screening of the proband revealed compound heterozygosity in the *SCN5A* gene. The paternal allele had two missense variants, leading to amino-acid substitutions of alanine by threonine in position 1924 (A1924T) and valine by methionine in position 1251 (V1251M). The variant V1251M is a benign polymorphism (Kapplinger et al., 2015). The maternal allele had an in-frame, single codon deletion, resulting in a removal of one out of two adjacent lysines, in positions 1492-1493 (K1493del) (**Figures 1B,C**). We cannot rule out the presence of mutation(s) in additional gene(s) that were not identified in the present gene screen.

Holter-testing of both parents did not reveal bradycardia, but the father displayed premature ventricular contractions (PVCs) with Right Bundle Branch Block (RBBB) pattern in V1 on 12-lead ECG. One brother did not have bradycardia. Another brother had bradycardia but he declined any clinical or genetic evaluation (**Figure 1D**).

Although K1493del and A1924T heterozygotes were previously reported with bradyarrhythmias (Rook et al., 1999; Zumhagen et al., 2013), the heterozygotes in this report were asymptomatic, probably due to reduced disease penetrance in these individuals. The extent and reasons for *SCN5A* mutation expression variability are not entirely clear. Reasons for the variability may include epigenetic gene silencing, age, gender, environmental factors and other genetic modifiers (Liu et al., 2016; Verkerk et al., 2018). We suggest that the accumulated effects in the compound-heterozygote may have increased the penetrance and severity of the arrhythmic phenotype compared with the heterozygotes in the reported family.

Complete Loss of $Na_V1.5$ Activity Due to K1493del Mutation, Without a Dominant-Negative Effect on Current Density

To examine the functional consequences of the variants, we expressed $Na_V1.5$, WT and mutants, in HEK cells and measured whole-cell I_{Na}. We used N-terminally GFP-fused $Na_V1.5$ that conserves the biophysical properties of $Na_V1.5$ (Clatot et al., 2012; Reinhard et al., 2013). Peak I_{Na} recorded in cells transfected with GFP-$Na_V1.5_{WT}$, with or without $Na_V\beta1$, was 1–6 nA. No I_{Na} was recorded in cells expressing GFP-$Na_V1.5_{K1493del}$

or the non-tagged $Na_V1.5_{K1493del}$. Addition of a bicistronic vector expressing $Na_V\beta1$ from two species (rat or human) together with RFP as an expression reporter did not recover I_{Na} (**Figure 2A**), even when the amount of DNA used for transfection of GFP-$Na_V1.5_{K1493del}$ +$Na_V\beta1$ was three-fold higher than GFP-$Na_V1.5_{WT}$. These results are at odds with a previous report (Zumhagen et al., 2013).

Compared with $Na_V1.5_{WT}$, the paternal variation $Na_V1.5_{A1924T*}$ did not affect I_{Na} density. In order to test whether $Na_V1.5_{K1493del}$ has a dominant-negative effect, GFP-$Na_V1.5_{K1493del}$ was added on top of $Na_V1.5_{WT}$ or $Na_V1.5_{A1924T*}$, in 1:1 DNA ratio. Co-expression of GFP-$Na_V1.5_{K1493del}$ did not reduce I_{Na} density, in HEK cells (**Figure 2B** and **Table 1**).

We used HL-1 cells, a mouse atrial cardiomyocyte tumor cell-line (Claycomb et al., 1998), to test the effect of $Na_V1.5_{K1493del}$ on endogenous cardiac-cell I_{Na}. HL-1 cells express sodium channel subunits, predominantly the $Na_V1.5$ α-subunit (Cerrone et al., 2014) and $Na_V\beta1$ subunit (**Figure 2Ca**), that recapitulate the physiological $Na_V1.5$ stoichiometry in a cardiac cell milieu. We transfected HL-1 cells with GFP-$Na_V1.5_{WT}$ or GFP-$Na_V1.5_{K1493del}$. Naïve, non-transfected, HL-1 cells showed I_{Na} of -144 ± 29 pA/pF. HL-1 cells transfected with GFP-$Na_V1.5_{WT}$ had I_{Na} of −594 ± 84 pA/pF, while cells transfected with GFP-$Na_V1.5_{K1493del}$ had a basal I_{Na} of −140 ± 32 pA/pF, similar to non-transfected cells.

These findings demonstrate, in HEK and HL-1 cells, that $Na_V1.5_{K1493del}$ is a loss-of-function mutant that does not induce a functional dominant-negative effect on I_{Na} density.

K1493del Attenuates $Na_V1.5$ Expression but Does Not Affect Trafficking

In order to understand if the basis for the loss-of-function in $Na_V1.5_{K1493del}$ was an impairment in the protein expression or trafficking to the plasma membrane, we performed a biotinylation assay. $Na_V1.5_{WT}$ and $Na_V1.5_{K1493del}$ were transfected in HEK cells. Total and plasma-membrane biotin-bound $Na_V1.5$ protein levels were quantified following Western-blot. We found a reduction in total cellular expression of $Na_V1.5_{K1493del}$ (40 ± 7% of $Na_V1.5_{WT}$). The % trafficking was determined by dividing the biotinylated fraction by total fraction, normalized to % trafficking of $Na_V1.5_{WT}$, in the same experiment. The % trafficking of $Na_V1.5_{K1493del}$ was not significantly different from % trafficking of $Na_V1.5_{WT}$ (93 ± 16%) so that a similar fraction from $Na_V1.5$ total protein was present at the plasma membrane (**Figures 3A,C**), suggesting that trafficking of $Na_V1.5_{K1493del}$ to the plasma membrane was not impaired.

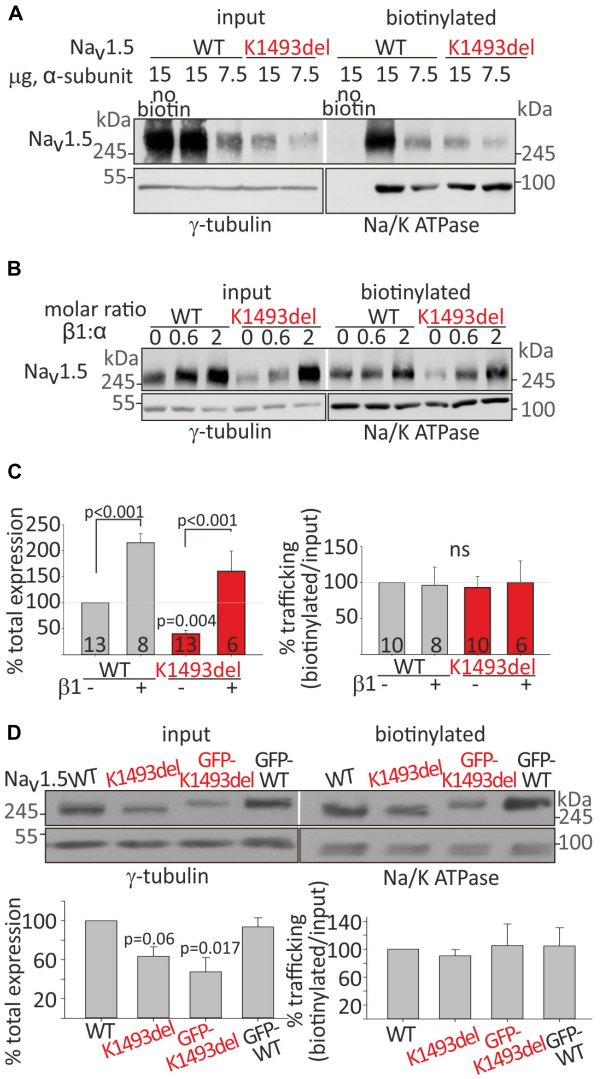

FIGURE 3 | Cell surface and total expression of $Na_V1.5_{WT}$ and $Na_V1.5_{K1493del}$. **(A,B)** Representative biotinylation assays. **(A)** HEK cells were transfected with $Na_V1.5_{WT}$ and $Na_V1.5_{K1493del}$. The control "no-biotin" group shows no signal from non-biotinylated channels. **(B)** HEK cells transfected with $Na_V1.5_{WT}$ and $Na_V1.5_{K1493del}$ (7.5 μg) +/– r$Na_V\beta1$ (2.5 and 7.5 μg). **(C)** Summary of % total protein (left) and % trafficking (right), normalized to $Na_V1.5_{WT}$ without $Na_V\beta1$. *N* = 9 experiments without $Na_V\beta$. *N* = 4 experiments with r$Na_V\beta1$ expressed. Groups expressing r$Na_V\beta1$ in molar ratios β:α 0.6-2 were pulled together. **(D)** GFP-fused and non-tagged $Na_V1.5_{WT}$ and $Na_V1.5_{K1493del}$ were expressed (without $Na_V\beta$ subunit). This is a summary of three experiments. Statistical significance was determined by one-way ANOVA, followed by Holm–Sidak test.

TABLE 1 | Current densities (pA/pF) of the normalized values presented in **Figure 2B**.

WT + GFP (*n* = 55)	−235 ± 22
GFP-WT (*n* = 14)	−220 ± 24
A1924T* + GFP (*n* = 39)	−247 ± 24
A1924T* + GFP-K1493del (*n* = 38)	−211 ± 18
WT + GFP-K1493del (*n* = 24)	−160 ± 16

$Na_V\beta1$ has been reported to improve the expression and trafficking of loss-of-function mutants of the sodium channel (Bechi et al., 2015). We examined the effect of $Na_V\beta1$ co-expression on total and cell-surface expression of $Na_V1.5_{WT}$ and $Na_V1.5_{K1493del}$. Addition of $Na_V\beta1$ enhanced total expression of both $Na_V1.5_{WT}$ and $Na_V1.5_{K1493del}$, with a concomitant increase in channel expression at the cell surface (**Figure 3B**).

A summary of total and biotinylated $Na_V1.5$ levels, normalized to the $Na_V1.5_{WT}$ expressed without $Na_V\beta1$ in the same experiment, is presented in **Figure 3C**. Co-expression of $Na_V\beta1$ increased total expression of $Na_V1.5_{WT}$ by 215 ± 18% and $Na_V1.5_{K1493del}$ by ∼400%, increasing the latter from 40 ± 7% to 160 ± 39% (compared to $Na_V1.5_{WT}$ without $Na_V\beta1$). $Na_V1.5_{K1493del}$ trafficking to the plasma membrane was similar to $Na_V1.5_{WT}$ when $Na_V\beta1$ was co-expressed. These results support the conclusion that K1493del does not affect forward-trafficking or $Na_V\beta1$-regulated trafficking and expression (**Figure 3A**).

To test whether the addition of a GFP-tag to $Na_V1.5$ N-terminus affected the expression or trafficking of $Na_V1.5$, we performed a biotinylation experiment on GFP-tagged and non-tagged channels. GFP-fusion did not change the biogenesis properties: total expression of GFP-$Na_V1.5_{K1493del}$ was partially reduced compared to GFP-$Na_V1.5_{WT}$, and GFP-tagged $Na_V1.5$ channels were exported to the plasma membrane (**Figure 3D**).

In summary, K1493del partially reduced total protein expression but did not affect the plasma-membrane trafficking of $Na_V1.5$. Co-expression of $Na_V\beta1$ restored the reduced $Na_V1.5_{K1493del}$ cellular levels but did not restore I_{Na} (**Figure 2A**), thus the loss-of-function by K1493del mutation is only marginally due to a biogenesis defect.

Expression of Non-conducting $Na_V1.5_{K1493del}$ and $Na_V\beta1$ Affects Ca^{2+}-Dependent Gating

We wanted to examine whether the non-conducting channel $Na_V1.5_{K1493del}$ affects the current of the co-expressed $Na_V1.5_{A1924T*}$ variant, consistent with the compound heterozygosity observed in the patient. We tested Ca^{2+}-dependent gating properties of I_{Na} in view of previous studies that included K1493 and A1924 residues in structural elements that bind the Ca^{2+}-sensor CaM: DIII-IV linker and the CT, respectively. When the I_{Na} conducting variants $Na_V1.5_{A1924T*}$ or $Na_V1.5_{WT}$ were co-expressed with the non-conducting variant $Na_V1.5_{K1493del}$, the latter was expressed as a GFP-fused channel to attest its co-expression in cells that displayed I_{Na}. Co-expression of GFP-$Na_V1.5_{K1493del}$ resulted in a 3 mV depolarizing shift of the activation curve of $Na_V1.5_{A1924T*}$ in the presence of [10 μM $Ca^{2+}]_{in}$ but not in the absence of $[Ca^{2+}]_{in}$. Co-expression of GFP-$Na_V1.5_{K1493del}$ with $Na_V1.5_{WT}$ resulted in a similar 3.5 mV depolarizing shift of the activation curve, only in [10 μM $Ca^{2+}]_{in}$ (**Figure 4A** and **Table 2**). Although modest, the depolarizing shift in the activation curve in the presence of Ca^{2+} was significant. The similar current amplitudes (**Table 2**) and the similar effect in the two unrelated groups argue against the possibility of a recording artifact being the reason for the observed shift.

As previously reported with $Na_V1.5_{A1924T}$ (Potet et al., 2009), the SSI curve of $Na_V1.5_{A1924T*}$ shifts to hyperpolarized voltages compared to $Na_V1.5_{WT}$, in the absence, but not in the presence, of $[Ca^{2+}]_{in}$. Co-expression of GFP-$Na_V1.5_{K1493del}$ caused a depolarizing shift of SSI of $Na_V1.5_{WT}$ and $Na_V1.5_{A1924T*}$ by 5.6 and 6.4 mV, respectively, in the absence of $[Ca^{2+}]_{in}$, but did not affect SSI properties in the presence of [10 μM $Ca^{2+}]_{in}$ (**Figure 4B** and **Table 2**). Recovery from inactivation induced by a 1 s depolarizing pulse was not affected by GFP-$Na_V1.5_{K1493del}$ co-expression (**Figure 4C** and **Table 2**).

To conclude, expression of non-conductive GFP-$Na_V1.5_{K1493del}$ altered the gating properties of co-expressed conducting channels, in a Ca^{2+}-dependent manner: a slight decrease in the voltage dependency of activation curve in [10 μM $Ca^{2+}]_{in}$, and an increase in $Na_V1.5$ availability following inactivation, in the absence of $[Ca^{2+}]_{in}$.

Since $Na_V1.5_{K1493del}$ plasma membrane expression was ∼40% of $Na_V1.5_{WT}$, and $Na_V\beta1$ enhanced $Na_V1.5_{K1493del}$ membrane expression (**Figure 3C**), we decided to examine the Ca^{2+}-dependent gating effects of functional channels ($Na_V1.5_{WT}$ or $Na_V1.5_{A1924T*}$) co-expressed with $Na_V\beta1$/RFP and GFP-$Na_V1.5_{K1493del}$.

$Na_V\beta1$ expression induced a Ca^{2+}-independent depolarizing shift in $Na_V1.5_{WT}$ SSI (Wingo et al., 2004), nevertheless, we observed a Ca^{2+}-dependent regulation of the activation. $Na_V\beta1$- expression induced a depolarizing shift in $Na_V1.5_{WT}$ activation curve, in the presence of [10 μM $Ca^{2+}]_{in}$ but not in the absence of $[Ca^{2+}]_{in}$ (**Table 2** and **Figure 4D**). A1924T* mutation eliminated $Na_V\beta1$-dependent effects on gating. Co-expression of $Na_V\beta1$ did not shift the activation or SSI curves of $Na_V1.5_{A1924T*}$, in either the absence or presence of $[Ca^{2+}]_{in}$ (**Figures 4D,E** and **Table 2**). The same effect was observed when 10 μM Ca^{2+} were chelated with HEDTA instead of BAPTA (**Figure 4E**).

Co-expression of GFP-$Na_V1.5_{K1493del}$ had no significant effect on activation or SSI curves of $Na_V1.5_{WT}$ +$Na_V\beta1$, in either the absence or presence of $[Ca^{2+}]_{in}$. Nevertheless, GFP-$Na_V1.5_{K1493del}$ co-expression right-shifted the SSI curve of $Na_V1.5_{A1924T*}$ + $Na_V\beta1$, only in the absence of $[Ca^{2+}]_{in}$ (**Figure 4F** and **Table 2**), similar to the effect recorded without $Na_V\beta1$ (**Figure 4B**). GFP-$Na_V1.5_{K1493del}$ co-expression did not significantly change the activation properties of $Na_V1.5_{A1924T*}$ + $Na_V\beta1$ (**Table 2**). Thus, the mutation A1924T* blunted $Na_V\beta1$-induced gating regulation and partially restored the effects that were induced by GFP-$Na_V1.5_{K1493del}$ co-expression.

We suggest that $Na_V\beta1$ directly affects $Na_V1.5$ Ca^{2+}-dependent gating in addition to its role in expression regulation. Our results demonstrate, for the first time, that $Na_V\beta1$-regulates $Na_V1.5$ gating in a Ca^{2+}-dependent manner, and that $Na_V\beta1$-induced regulation mechanism includes the A1924 residue. In summary, $Na_V1.5$ Ca^{2+}-sensitivity involves multiple elements, including both CaM-interacting elements: CT and DIII-IV, and possibly a protein complex that includes more than one $Na_V1.5$ channel.

K1493del Mutation Modulates CaM-$Na_V1.5$ Interaction

We wanted to examine CaM-interaction with $Na_V1.5$ variants, since CaM directly interacts with $Na_V1.5$ at the two domains where variants were found in the proband: A1924T located in the conserved IQ-domain in the cytoplasmic CT (Gabelli et al., 2014; Wang et al., 2014), and K1493del in the proximal segment of the cytoplasmic DIII-IV linker (Potet et al., 2009; Sarhan et al., 2012; Johnson et al., 2018; **Figure 1C**). We explored the interactions of

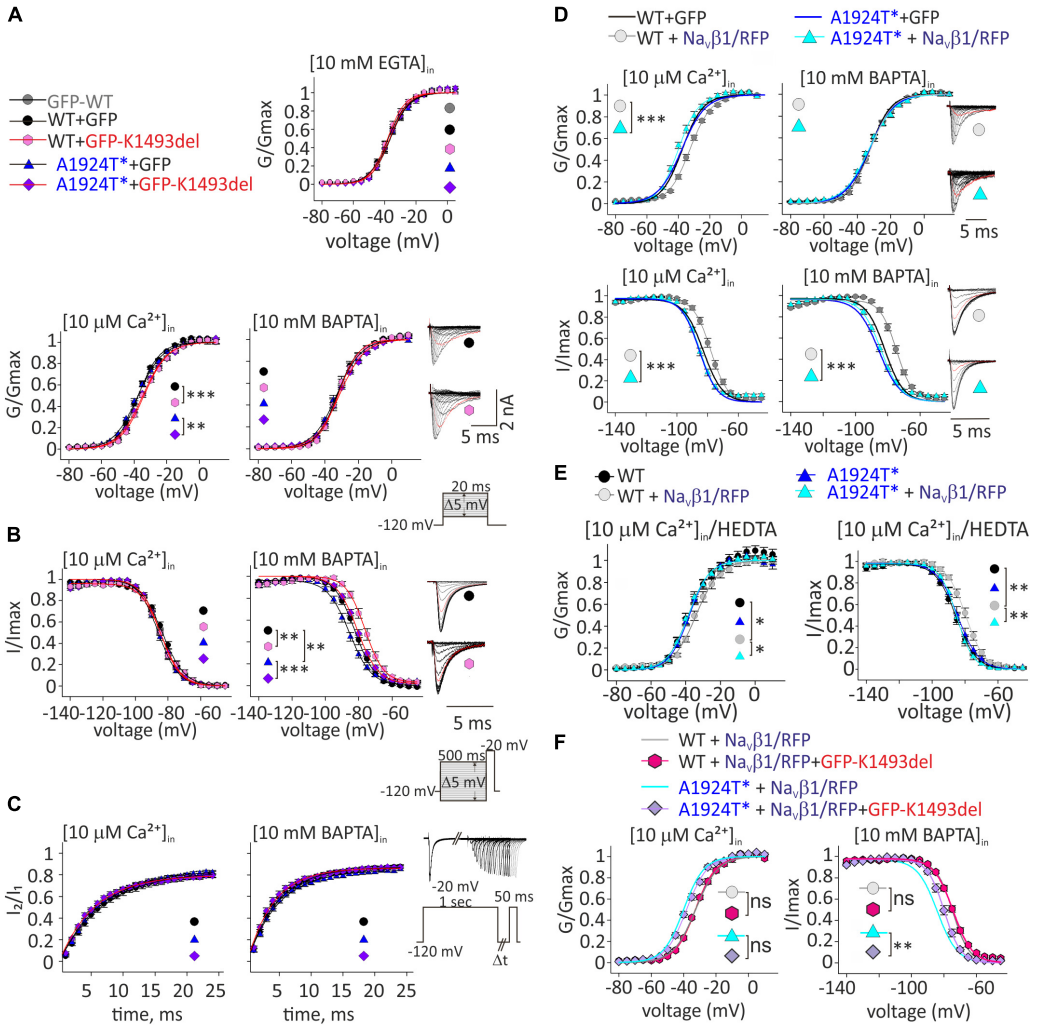

FIGURE 4 | Ca^{2+}-dependent gating properties of $Na_V1.5$ variants. **(A)** Activation curves of conductance-voltage relationship. Current traces recorded in [10 µM $Ca^{2+}]_{in}$, and –40 mV trace is red. **(B)** SSI curves of voltage-dependent channel availability. Current traces during the test pulse at –20 mV are with (10 mM BAPTA)$_{in}$. The test-pulse trace that follows –80 mV pre-pulse is red. **(C)** Recovery from inactivation. **(D)** Activation (top) and SSI (bottom) curves of $Na_V1.5_{WT}$ +GFP and $Na_V1.5_{A1924T*}$ +GFP co-expressing r$Na_V\beta1$/RFP were plotted with the fitted curves of these groups without r$Na_V\beta1$/RFP (presented in **A**, **B**). Current traces recorded in [10 µM $Ca^{2+}]_{in}$. The –40 mV trace during activation and the test-pulse that follows the –80 mV pre-pulse during SSI are red. **(E)** Activation (left) and SSI (right) curves with 10 µM Ca^{2+} chelated with HEDTA in the internal solution. **(F)** Activation (left) and SSI (right) curves of $Na_V1.5$ variants co-expressing r$Na_V\beta1$/RFP and GFP-$Na_V1.5_{K1493del}$ were plotted with the fitted curves of these groups without GFP-$Na_V1.5_{K1493del}$ (presented in **D**). Statistical significance of Va was determined by *t*-test: ns, not significant;*$p < 0.05$; **$p < 0.01$; ***, $p < 0.001$ (see **Table 2**).

CaM with $Na_V1.5$ expressed in HEK cells by a pull-down essay using CaM-coated agarose beads.

CaM interaction in the presence of 2 mM Ca^{2+} (Ca^{2+}/CaM interaction) and in the absence of Ca^{2+} (apo-CaM interaction in 10 mM EGTA) with $Na_V1.5_{WT}$ and mutants in the same experiment, were normalized to Ca^{2+}/CaM-$Na_V1.5_{WT}$ interaction. Co-expression of $Na_V\beta1$ enabled comparable protein expression levels of $Na_V1.5_{K1493del}$ and $Na_V1.5_{WT}$. A three-fold reduction in CaM-$Na_V1.5_{WT}$ interaction in the absence of Ca^{2+} (from 100% with Ca^{2+} to 35 ± 13% without Ca^{2+}), and a two-fold reduction in CaM-$Na_V1.5_{A1924T*}$ interaction in the absence of Ca^{2+} (from 108 ± 8% with Ca^{2+} to 51 ± 6% without Ca^{2+}) were observed (**Figure 5A**). Ca^{2+}/CaM interaction with $Na_V1.5_{K1493del}$ were strongly reduced (20 ± 5% of $Na_V1.5_{WT}$). The Ca^{2+}/CaM and apo-CaM interaction with $Na_V1.5_{K1493del}$ were not significantly different, indicating an impaired Ca^{2+}-dependent interaction (**Figure 5A**).

CaM co-expression enhanced total-expression of $Na_V1.5_{WT}$ by 161 ± 18% and $Na_V1.5_{K1493del}$ by 387 ± 93% (**Figures 5Ba,b**), suggesting that despite a reduction in Ca^{2+}/CaM interaction, CaM regulates the expression levels of $Na_V1.5_{K1493del}$. Upregulation of $Na_V1.5_{K1493del}$ expression in the presence of over-expressed CaM enabled quantification of CaM-$Na_V1.5_{K1493del}$ interaction. The ratio of $Na_V1.5$ bound-to-input levels in 2 mM Ca^{2+} was lower in $Na_V1.5_{K1493del}$ compared to $Na_V1.5_{WT}$ (58 ± 10%, **Figures 5Ba,c**). Thus, CaM

TABLE 2 | Gating properties of $Na_V1.5$ in different Ca^{2+} chelation.

		10 mM EGTA																					
		WT + GFP			GFP-WT			A1924T* +GFP			A1924T* +GFP-K1493del			WT + GFP-K1493del			GFP-WT + rβ1			GFP-WT + hβ1		
		mean	*n*	SEM	mean	*n*	SEM	mean	*n*	SEM	mean	*n*	SEM	mean	*n*	SEM	mean	*n*	SEM	mean	n	SEM
activation	Gmax	46.8	18	7.0	47.0	14	6.18	51.7	9	8.9	74.8	7	7.2	38.5	10	6.2	57.94	10	9.25	51.4	12	5.6
	Vrev	42.0	18	2.5	48.8	14	3.0	31.0	9	2.0	35.2	7	3.7	41.6	10	1.7	35.83	10	5.6	34.4	12	4.2
	Va	−36.8	18	1.0	−38.7	14	0.98	−36.8	9	0.9	−36.8	7	1.0	−38.1	10	0.8	−37.8	10	2.5	−39.5	12	2.35
	Ka	6.15	18	0.3	6.23	14	0.3	6.4	9	0.4	5.6	7	0.2	5.5	10	0.4	6.2	10	0.7	5.6	12	0.54

		10 μM Ca^{2+} (using BAPTA)												0 Ca^{2+} (10 mM BAPTA)									
		WT + GFP			WT + GFP-K1493del			A1924T* + GFP			A1924T* + GFP-K1493del			WT + GFP			WT + GFP-K1493del			A1924T* + GFP			A1924T* + GFP-K1493del		
		mean	n	SEM	mean	n	SEM	mean	n	SEM	mean	n	SEM	mean	n	SEM	mean	n	SEM	mean	n	SEM	mean	n	SEM
activation	Gmax	49.5	13	8.1	46.4	15	6.4	47.4	7	9.6	52.8	22	6.0	73.2	7	10.8	45.1	7	8.9	53.2	15	7.7	36.8	16	3.9
	Vrev	42.4	13	1.9	46.2	15	4.2	40.1	7	2.2	45.4	22	2.6	51.0	7	1.2	57.8	7	6.1	54.0	15	2.0	58.1	16	2.1
	Va	−37.6	13	0.6	−34.1[a]	15	0.6	−37.8	7	0.7	−34.8[b,c]	22	0.5	−32.2	7	1.3	−31.7	7	1.2	−32.6	15	0.7	−31.0	16	0.5
	Ka	6.4	13	0.3	7.2	15	0.3	7.5	7	0.4	7.4	22	0.3	5.9	7	0.4	5.8	7	0.5	7.2	15	0.4	7.4	16	0.4
Amplitude (pA)		−2872	13	502	−2521	15	323	−2583	7	532	−2836	22	308	−4509	7	647	−3002	7	578	−3330	15	513	−2523	16	230
SSI	Va	−83.8	20	0.8	−83.8	5	0.8	−86.0	15	0.7	−85.2	10	0.8	−81.7	29	1.0	−76.1[d]	10	1.2	−86.2[e]	24	1.2	−79.8[f]	22	0.9
	Ka	6.3	20	0.4	7.0	5	0.8	5.7	15	0.2	5.9	10	0.2	5.0	29	0.1	5.3	10	0.2	5.8	24	0.2	5.6	22	0.2
Rec. IA	A	0.87	16	0.02				0.86	15	0.02	0.80	9	0.02	0.88	18	0.02				0.85	18	0.02	0.87	13	0.01
	τ	7.1	16	0.4				7.2	15	0.5	5.7	9	0.2	5.1	18	0.4				5.1	18	0.4	4.4	13	0.4

a, $p < 0.001$ compared to WT+ GFP; b, $p = 0.009$ compared to A1924T+ GFP; c, $p = 0.003$ compared to WT+ GFP; d, $p = 0.005$ compared to WT+ GFP; e, $p = 0.006$ compared to WT+ GFP; f, $p < 0.001$ compared to A1924T*+ GFP.*

(Continued)

TABLE 2 | Continued

		10 μM Ca^{2+} (using BAPTA)												0 Ca^{2+} (10 mM BAPTA)									
		WT + rβ1			WT + GFP-K1493del + rβ1			A1924T* + rβ1			A1924T* + GFP-K1493del + rβ1			WT + rβ1			WT + GFP-K1493del + rβ1			A1924T* + rβ1			A1924T* + GFP-K1493del + rβ1		
		mean	n	SEM	mean	n	SEM	mean	n	SEM	mean	n	SEM	mean	n	SEM	mean	n	SEM	mean	n	SEM	mean	n	SEM
activation	Gmax	39.2	11	4.6	44.7	6	6.8	68.5	6	10.5	75.6	8	11.9	63.9	20	5.13	59.2	9	8.2	38.0	11	6.0	52.5	12	8.0
	Vrev	46.8	11	2.0	51.6	6	4.2	43.0	6	1.0	38.1	8	2.2	50.6	20	1.76	52.2	9	1.8	50.4	11	1.5	52.2	12	2.0
	Va	−32.6[g]	11	0.6	−32.6	6	0.5	−39.9[h]	6	0.9	−37.9	8	0.9	−31.9	20	0.8	−30.7	9	0.4	−31.7	11	0.7	−32.1	12	0.6
	Ka	6.9	11	0.4	6.4	6	0.6	6.2	6	0.5	6.7	8	0.3	6.1	20	0.3	6.7	9	0.4	7.7	11	0.3	7.5	12	0.5
Amplitude (pA)		−2248	11	290	−2789	6	349	−4270	6	704	−4043	8	670	−3836	20	314	−3548	9	484	−2187	11	356	−3124	12	476
SSI	Va	−78.0[i]	12	0.9	−76.6	10	0.7	−86.3[j]	6	0.8	−85.2	6	1.3	−74.5[k,l]	15	0.7	−74.1	13	0.7	−83.2[m]	11	0.9	−78.5[n]	15	1.0
	Ka	5.2	12	0.3	5.3	10	0.3	5.0	6	0.3	4.9	6	0.3	4.8	15	0.2	5.6	13	0.2	5.25	11	0.3	4.91	15	0.1

g, $p < 0.001$ compares to WT+ GFP; h, $p < 0.001$ compares to WT+rβ1; i, $p < 0.001$ compares to WT+ GFP; j, $p < 0.001$ compares to WT+rβ1; k, $p = 0.007$ compared to WT+rβ1 in 10 μM Ca^{2+}; l, $p < 0.001$ compares to WT+ GFP; m, $p < 0.001$ compares to WT+rβ1; n, $p = 0.003$ compared to A1924T+rβ1.*

		10 μM Ca^{2+} (using HEDTA)											
		WT			WT + rβ1			A1924T*			A1924T* + rβ1		
		mean	n	SEM	mean	n	SEM	mean	n	SEM	mean	n	SEM
activation	Gmax	75.5	10	8.8	46.9	10	8.1	57.2	5	18.4	73.8	5	17.8
	Vrev	45.0	10	2.3	40.7	10	3.2	48.8	5	3.1	44.2	5	1.4
	Va	−37.2	10	1.0	−33.7[o]	10	1.2	−37.9	5	0.8	−38.4[p]	5	1.4
	Ka	6.3	10	0.2	6.9	10	1.0	5.7	5	0.4	5.8	5	0.6
Amplitude (pA)		−4633	10	507	−2880	10	547	−3764	5	1241	−4622	5	1192
SSI	Va	−85.6	6	1.3	−80.1[q]	5	0.9	−84.4	7	1.7	−85.1[r]	7	1.1
	Ka	6.0	6	0.4	6.4	5	0.7	5.8	7	0.5	4.8	7	0.1

o, $p = 0.037$ compared to WT; p, $p = 0.033$ compared to WT+rβ1; q, $p = 0.007$ compared to WT; r, $p = 0.008$ compared to WT+rβ1. SSI, steady-state inactivation; rec IA, recovery from inactivation. Significance between two groups was tested using a two-tailed t-test, in the same solution unless otherwise mentioned. β subunits were expressed with RFP in the same vector (β1/RFP).

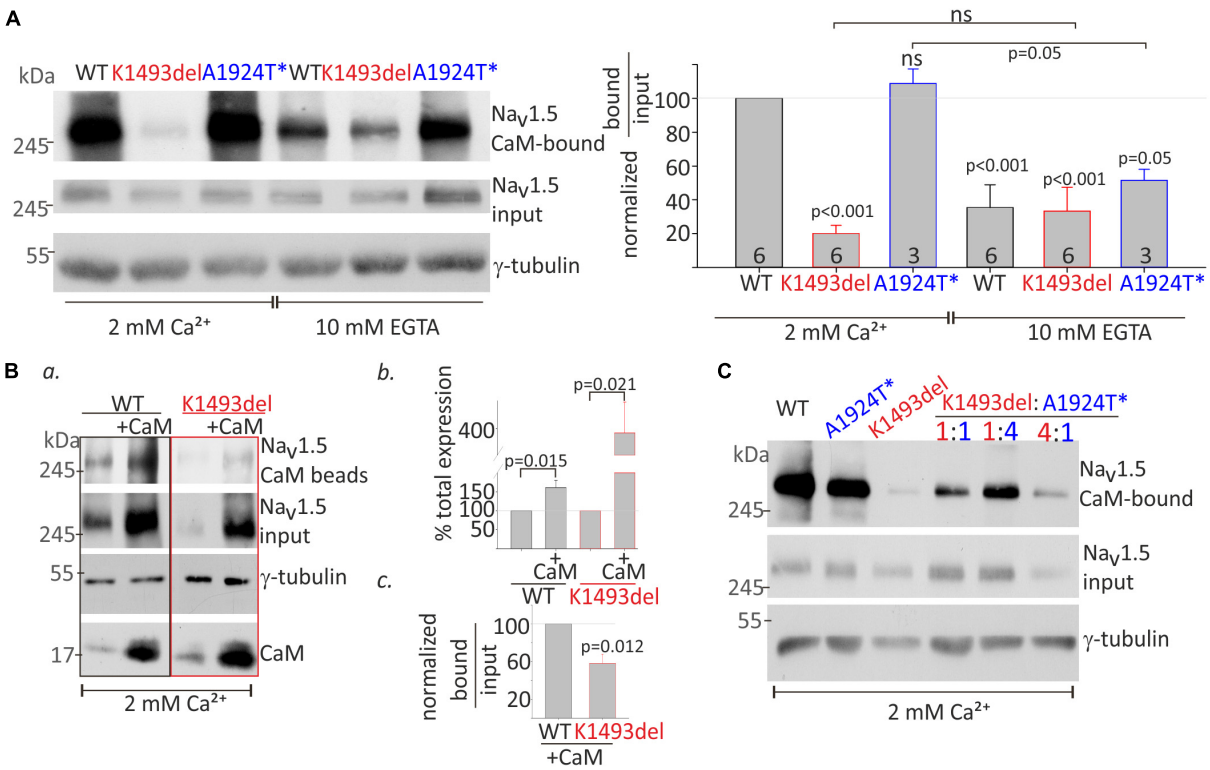

FIGURE 5 | CaM-interaction with $Na_V1.5$ variants **(A)**. HEK cells were transfected with $Na_V1.5_{WT}$, $Na_V1.5_{K1493del}$, and $Na_V1.5_{A1924T*}$ together with $rNa_V\beta1$. Lysates from transfected groups were pulled-down with CaM-agarose beads in Ca^{2+} and EGTA. Left, a representative Western blot from a pull-down assay. Right, the CaM-bound fraction was normalized to input level, and presented as % of $Na_V1.5_{WT}$ in 2 mM Ca^{2+}, in the same experiment. Statistical significance was determined by one-way ANOVA followed by Holm–Sidak test. *P*-value compared to $Na_V1.5_{WT}$ in 2 mM Ca^{2+} is indicated above each bar. **(B)** $Na_V1.5_{WT}$ and $Na_V1.5_{K1493del}$ with or without co-expressed CaM were pulled-down with CaM-agarose beads in 2 mM Ca^{2+}. **(a)** CaM- bound $Na_V1.5$, and total input levels of $Na_V1.5$, CaM and γ-tubulin were detected in Western-blot. **(b)** Input $Na_V1.5$+CaM levels were normalized to $Na_V1.5$ without CaM, from the same experiment, $N = 4$. **(c)** CaM-bound fractions were normalized to input levels, and are presented as % of $Na_V1.5_{WT}$+CaM in the same experiment, $N = 3$. Statistical significance was estimated by *t*-test. **(C)** HEK cells transfected with equal total $Na_V1.5$ α-subunit (7.5 μg; ratio 1:1, 3.75 μg of each construct; ratio 1:4, 1.5, and 6 μg of the constructs indicated) together with $rNa_V\beta1$. Lysates from transfected groups were pulled-down with CaM-agarose beads in 2 mM Ca^{2+}. This is a representative experiment out of two.

over-expression was not able to fully restore the reduction in Ca^{2+}/CaM-$Na_V1.5_{K1493del}$ interaction.

We wanted to determine whether the combination of the two mutated channels, as presented in the patient, affects the overall binding of the expressed channels to CaM. We hypothesized that a cross-talk between $Na_V1.5$ proteins would result in cooperative CaM-interaction and that reduced Ca^{2+}/CaM-interaction in $Na_V1.5_{K1493del}$ would interfere with overall Ca^{2+}/CaM-interaction. Our results did not support this hypothesis. The extent of overall channel binding to CaM beads in 2 mM Ca^{2+} varied proportionally to the ratio of expressed $Na_V1.5_{K1493del}$ and $Na_V1.5_{A1924T*}$: the more $Na_V1.5_{K1493del}$ – the less overall CaM binding (**Figure 5C**).

The Mechanism of $Na_V1.5_{K1493del}$ Loss-of-Function

The lysine doublet in position 1492-3 is positively charged and is located in a region rich with polar and charged residues that could potentially contribute to protein-protein interactions (**Figure 6A**). These residues are located in a conserved helical structure, downstream of the IFM motif that confers fast inactivation (West et al., 1992). We hypothesized that a salt-bridge could affect channel function and CaM interaction. To test this, we created three $Na_V1.5$ mutants, where the lysine in position 1493 was mutated to the neutral residue alanine, $Na_V1.5_{K1493A}$, the negative residue glutamate, $Na_V1.5_{K1493E}$, or another positive residue, arginine, $Na_V1.5_{K1493R}$.

Analysis of $Na_V1.5$ currents revealed that all three mutated channels were functional (**Figures 6Ba,b**). However, inactivation properties were altered. Using a single-exponential fit to estimate the inactivation time constant, τ, we found that when the positive charge in residue 1493 was conserved (K1493R), inactivation rate was similar to WT, as previously reported (Li et al., 2009). However, the inactivation rate was increased when K1493 was changed to an uncharged or a negatively charged residue (K1493A/E, respectively, **Figure 6Bc**). These results indicate that the electric charge in position 1493 is important for fast-inactivation kinetic properties, but not for the total function.

Expression analysis showed that the total protein levels of the three mutants $Na_V1.5_{K1493A/E/R}$ were not significantly

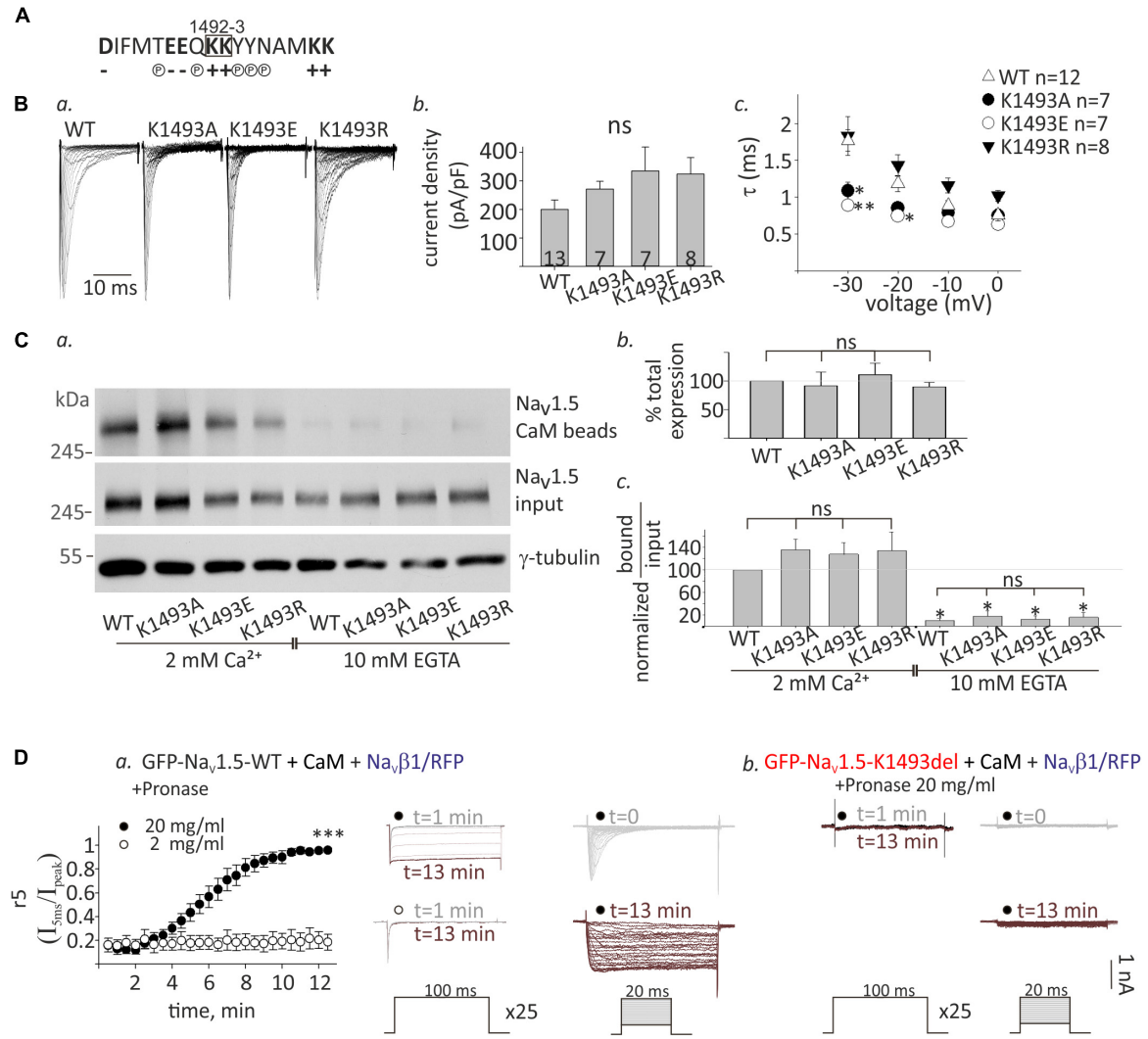

FIGURE 6 | Functional and biochemical role of K1493 residue. **(A)** The amino acid sequence of residues 1484–1500 in $Na_V1.5$. The double lysines 1492-3 are marked in a square. Amino acid's charge (+ or–) or polarity (P) are indicated. **(B)** $Na_V1.5$ variants co-expressed with $rNa_V\beta1$. **(a)** Representative I_{Na} traces recorded in $(10\ mM\ EGTA)_{in}$. **(b)** Maximal current densities. **(c)** Time constant (τ) obtained by fitting a single exponential to the decay phase of the currents in $(10\ mM\ EGTA)_{in}$ at four voltages. Statistical significance was determined by one-way ANOVA followed by Holm–Sidak test (compared to $Na_V1.5_{WT}$). **(C)** Cells were transfected with $Na_V1.5_{K1493A/E/R}$ together with $rNa_V\beta1$. **(a)** Example of a pull-down experiment with CaM-agarose beads, in Ca^{2+} and EGTA. **(b)** The total expression as quantified in EGTA, and normalized to $Na_V1.5_{WT}$ ($N = 3$). **(c)** Pull-down experiments with CaM-agarose beads. The CaM-bound fraction was normalized to input level and quantified as % of $Na_V1.5_{WT}$ in 2 mM Ca^{2+} ($N = 3$). Statistical significance was determined by one-way ANOVA, followed by Holm–Sidak test, compared to WT in 2 mM Ca^{2+}. $^{**}p < 0.01$; $^{*}p < 0.05$. **(D)** GFP-$Na_V1.5_{WT}$ **(a)** or GFP-$Na_V1.5_{K1493del}$ **(b)** coexpressed with $rNa_V\beta1$/RFP and CaM in HEK cells. 2 or 20 mg/ml pronase were added to $(10\ mM\ EGTA)_{in}$ pipette solution. *t* indicates the time from the beginning of the recording. **(a)** Currents elicited from –120 mV to –20 mV for 100 ms, every 30 s. Between pulses, the cells were held at –120 mV. Inactivation was evaluated by r_5, which is the fraction of current that remained after 5 ms at –20 mV (I_{5ms}/I_{peak}), $n = 5$ in each group (left). Representative currents during repetitive steps to –20 mV (middle), and activation protocols in the same cell, at different time points (right). **(b)** Recording from cells expressing GFP-$Na_V1.5_{K1493del}$ with 20 mg/ml pronase in the pipette solution. Currents during repetitive depolarization (left) and activation protocols (right) at different time points are presented. This is a representative cell out of 12 cells.

different from $Na_V1.5_{WT}$ (**Figures 6Ca,b**). CaM-interaction with $Na_V1.5_{K1493A/E/R}$ was Ca^{2+}-dependent, similar to $Na_V1.5_{WT}$ (**Figures 6Ca,c**). This set of experiments demonstrates that, unlike the robust effect of the K1493 deletion mutation, the biochemical and functional characteristics of $Na_V1.5$ are not highly dependent on the electric charge in K1493 residue.

We further explored the mechanism of $Na_V1.5_{K1493del}$ loss-of-function in view of the mutation location, in $Na_V1.5$ inactivation gate. We hypothesized that $Na_V1.5_{K1493del}$ is constitutively inactivated resulting in a channel-pore block. To address this hypothesis, we used the protease pronase that selectively destroys the inactivation of sodium channels while leaving activation intact (Armstrong et al., 1973). HEK cells were transfected with GFP-$Na_V1.5_{WT}$ or GFP-$Na_V1.5_{K1493del}$ together with both CaM and $Na_V\beta1$/RFP to allow maximal expression of $Na_V1.5$ variants. Dialysis of 20 mg/ml pronase

into the cell through the patch pipette gradually relieved the inactivation of $Na_V1.5_{WT}$ I_{Na} until its complete elimination after 12 min. The effect on I_{Na} inactivation was dose-dependent and 2 mg/ml pronase did not eliminate the inactivation in 12 min (**Figure 6Da**). Cells expressing GFP-$Na_V1.5_{K1493del}$ and $Na_V\beta1$/RFP in addition to CaM had no I_{Na}. Dialysis of 20 mg/ml pronase, in the same protocol used for $Na_V1.5_{WT}$, did not restore $Na_V1.5_{K1493del}$ current. We conclude that the reasons for $Na_V1.5_{K1493del}$ loss-of-function are beyond a change in the inactivation properties, and probably involve structural and additional functional perturbations.

DISCUSSION

Sinus-bradycardia and cardiac conduction-disease in the proband were associated with novel heterozygous *SCN5A* variants composition, K1493del in DIII-IV linker and A1924T* in the CT of $Na_V1.5$. Deletion of K1493 caused a complete loss of $Na_V1.5$ function. Surprisingly, the expression of the non-conducting $Na_V1.5_{K1493del}$ affected Ca^{2+}-dependent gating properties of co-expressed conducting channels. Moreover, Ca^{2+}-dependent CaM-$Na_V1.5$ interaction was impaired in $Na_V1.5_{K1493del}$. A Ca^{2+}-dependent $Na_V\beta1$ modulation that was characterized in $Na_V1.5_{WT}$ currents, was impaired in the $Na_V1.5_{A1924T*}$ variant. These results highlight the significance of $Na_V1.5$ DIII-IV linker in channel function and CaM-interaction and suggest that the Ca^{2+}-sensing machinery of $Na_V1.5$ involves $Na_V\beta1$ and more than one monomeric $Na_V1.5$ channel.

Function and Biogenesis of $Na_V1.5_{K1493del}$

Sodium channelopathies usually occur due to disruption of two mechanisms: gating and/or biogenesis, a process that includes synthesis, folding, assembly of the macromolecular complex, trafficking to the plasma membrane and localization in cell surface compartments (Chen-Izu et al., 2015). Co-expression of the auxiliary proteins $Na_V\beta1$ and CaM increased $Na_V1.5_{WT}$ and $Na_V1.5_{K1493del}$ total expression (**Figures 3B**, **5Bb**), possibly by serving as chaperons, suggesting a proper biogenesis regulation of $Na_V1.5_{K1493del}$ by these proteins. The $Na_V\beta1$ and the ubiquitous CaM are expressed throughout the heart and the cardiac conduction system (O'malley and Isom, 2015). Thus, we assume that expression levels of $Na_V1.5_{K1493del}$ in the human heart are close to the physiological levels of $Na_V1.5_{WT}$.

The non-conducting channel $Na_V1.5_{K1493del}$ did not exert a dominant-negative effect on the macroscopic current density of $Na_V1.5_{WT}$ or $Na_V1.5_{A1924T*}$ in HEK cells, or on endogenous I_{Na} of HL-1 atrial cells. Hence, $Na_V1.5_{K1493del}$ does not impair biogenesis of other sodium channels, a mechanism reported in other $Na_V1.5$ mutants (Keller et al., 2005; Clatot et al., 2012; Hoshi et al., 2014).

Deletion of K1493 resulted in a loss of I_{Na}. Changing K1493 electrostatic properties did not reduce I_{Na} but only modified inactivation kinetics (**Figure 6B**). Based on the location of the mutation in the inactivation gate, a constitutive inactivation state could account for $Na_V1.5_{K1493del}$ loss-of-function. However, pronase, a protease that relieves the inactivation of sodium channels following the digestion of DIII-IV linker (Stühmer et al., 1989), did not restore $Na_V1.5_{K1493del}$ currents (**Figure 6D**). Possible explanations are, first, that K1493del mutation altered $Na_V1.5$ DIII-IV linker conformation to hinder the access of pronase to its target sequence. In an inactivated state, the IFM motif acts as a latch of a hinged-lid that docks within the pore. If K1493del does not allow a release of the latch in resting potentials, then the channel remains locked in an inactivated state, and the substrate of pronase might not be exposed to the cytoplasm. A second possible explanation is that K1493 deletion not only destabilized the inactivation gate but also lead to a major deformation that obstructed the pore's cytosolic mouth. In this case, a twisted DIII-IV linker conformation results in a global interference in the protein structure and distal interaction with other $Na_V1.5$ cytosolic elements. Both options imply that the lysines in position 1492-3 are pivotal residues in $Na_V1.5$ gate and that removal of one lysine alters fundamental functional and structural elements in the channel gate.

Unlike a previous report (Zumhagen et al., 2013), we were unable to record I_{Na} in HEK cells expressing $Na_V1.5_{K1493del}$. In the previous and the current reports, $Na_V1.5_{K1493del}$ was expressed in HEK cells, and the patch-clamp solutions and experimental conditions were essentially similar. We tested several mechanisms that may have contributed to the discrepancy: (1) Impaired cellular expression: total and surface expression of $Na_V1.5_{K1493del}$ was confirmed by Western blot and biotinylation assay (**Figure 3**). (2) Low transfection of $Na_V1.5$ α-subunit: currents were measured in cells expressing GFP-labeled α-subunit ($Na_V1.5_{WT}$ and $Na_V1.5_{K1493del}$), and the amount of DNA used for transfection of $Na_V1.5_{K1493del}$ was three-fold higher. (3) Functional variability between $Na_V\beta1$ species: $Na_V\beta1$ subunit from two species were used (rat and human; the human $Na_V\beta1$ was previously used). (4) Low expression of $Na_V\beta1$ subunit: $Na_V\beta1$ was co-expressed with a fluorescent marker in a bicistronic vector. (5) Finally, the coding sequences of the constructs were fully sequenced, and two separately constructed α-subunit mutants ($Na_V1.5_{K1493del}$ and GFP-$Na_V1.5_{K1493del}$) were tested. In summary, our results show that $Na_V1.5_{K1493del}$ is a loss-of-function mutation due to a gating rather than a biogenesis defect, and the reason for the discrepancy with the previous report could not be determined.

DIII-IV Linker Mediates Ca^{2+}-Dependent $Na_V1.5$-CaM Interaction

The Ca^{2+}-sensing machinery of $Na_V1.5$ may include the DIII-IV linker, CT and the Ca^{2+} sensor CaM. Interaction of CaM with DIII-IV linker was studied mainly using small peptides (Kim et al., 2004; Potet et al., 2009; Sarhan et al., 2012; Yan H. et al., 2017; Johnson et al., 2018), but the relevance of DIII-IV linker to the overall CaM-binding complex in the full $Na_V1.5$ protein is unclear. The binding affinities of $Na_V1.5$-CT peptide to CaM were not Ca^{2+}-sensitive (Wang et al., 2014), while Ca^{2+}-dependent enhancement in CaM binding was measured with DIII-IV linker segments (Sarhan et al., 2009; Sarhan et al., 2012; Johnson et al., 2018). We detected a novel property of

CaM interaction with full $Na_V1.5$ expressed in cells: Ca^{2+}/CaM was stronger than apo-CaM interaction, in $Na_V1.5_{WT}$ and the variants $Na_V1.5_{A1924T*}$ (**Figure 5A**) and $Na_V1.5_{K1493A/E/R}$ (**Figure 6C**) when using pull-down assay. K1493del blunted the Ca^{2+}-dependent CaM-interaction: Ca^{2+}/CaM-$Na_V1.5_{K1493del}$ interaction was similar to apo-CaM-interaction with $Na_V1.5_{WT}$ or $Na_V1.5_{K1493del}$. These results highlight the role of DIII-IV linker in CaM binding complex, suggesting that the Ca^{2+}-dependent CaM-interaction with $Na_V1.5$ DIII-IV linker contributes, directly or indirectly, to the overall enhancement in Ca^{2+}/CaM-$Na_V1.5$ interaction.

The $Na_V1.5$ Mutation A1924T Does Not Eliminate Ca^{2+}-Dependent CaM-Interaction

A1924T mutation reduced Ca^{2+}/CaM-interaction in a CT peptide (Wang et al., 2014). However, the length of $Na_V1.5$ CaM-interacting segments was shown to be crucial for determining binding affinities to CaM [(Wang et al., 2014; Johnson et al., 2018) vs. (Sarhan et al., 2012)]. When we pulled-down the full-length expressed $Na_V1.5$, the interaction between Ca^{2+}/CaM and $Na_V1.5_{A1924T*}$ was not weakened compared to $Na_V1.5_{WT}$, unlike the reports in CT segments. However, in the absence of Ca^{2+}, $Na_V1.5_{A1924T*}$-CaM interaction was slightly higher compared to $Na_V1.5_{WT}$, so the "net" Ca^{2+}-dependent change in CaM interaction was diminished. Our results point that the binding of CaM to a native $Na_V1.5$ channel is probably determined by multiple segments, e.g., both the CT and the DIII-IV linker. CaM affinities to separate segments may not reflect the full dynamic interaction. Understanding the mode of integration of all $Na_V1.5$-CaM binding elements within the complete channel protein is indispensable for resolving the mechanism of CaM-regulation in a physiological context. Pioneering cryogenic electron microscopy (cryo-EM) studies were able to capture the cytosolic complex of sodium channels (Shen et al., 2017; Yan Z. et al., 2017), and together with functional and molecular information the understanding of the complex and dynamic Ca^{2+}-dependent regulation will be refined.

$Na_V1.5$ Gating Is Ca^{2+}-Dependent

Several studies demonstrated that $Na_V1.5$ is regulated by Ca^{2+} (Deschenes et al., 2002; Tan et al., 2002; Kim et al., 2004; Wingo et al., 2004; Biswas et al., 2009; Glynn et al., 2015; Gabelli et al., 2016; Abdelsayed et al., 2017), but the molecular details and the physiological relevance remains highly controversial [e.g. (Ben-Johny et al., 2014)]. We showed that $Na_V1.5_{K1493del}$ is located in the plasma membrane as a non-conducting channel. If individual $Na_V1.5$ monomers gate independently of others, the "silent" mutant $Na_V1.5_{K1493del}$ would not have contributed to overall macroscopic current properties when expressed with other channels in the same cell. Strikingly, expression of the non-conducting mutant channel affected the Ca^{2+}-dependent gating of macroscopic current arising from co-expressed conducting channels. Co-expression of $Na_V1.5_{K1493del}$ similarly altered the Ca^{2+}-dependent gating properties of both $Na_V1.5_{WT}$ and $Na_V1.5_{A1924T*}$: a depolarization shift in the voltage-dependent activation with $[Ca^{2+}]_{in}$ and SSI-curve in the absence of $[Ca^{2+}]_{in}$.

Previous studies provided evidence that $Na_V1.5$ proteins are in physical proximity when expressed in cells (Clatot et al., 2012; Mercier et al., 2012; Clatot et al., 2018). This interaction is indirect, via 14-3-3 protein (Clatot et al., 2017). Functional cooperation of the gate has been demonstrated when loss-of-function $Na_V1.5$ mutant impaired $Na_V1.5_{WT}$ gating by a dominant-negative mechanism (Clatot et al., 2018) while several other mutations showed a dominant-negative effect via defective biogenesis that suggests co-trafficking of several channels [reviewed in (Sottas and Abriel, 2016)]. Here, the expression of $Na_V1.5_{K1493del}$ did not cause a dominant-negative loss-of-function effect (**Figures 2B,C**). We propose that the loss of Ca^{2+}/CaM-interaction due to K1493del mutation prompted changes in the Ca^{2+}-dependent gating of co-expressed conducting channels. Thus, our results support a cooperative gating regulation of multimeric-$Na_V1.5$ complex and suggest that this mechanism involves a Ca^{2+}/CaM-regulated component. To note, CaM plays a critical role in the functional coupling of the structurally homologous calcium channel, $Ca_V1.2$ (Dixon et al., 2015). In summary, the mutation K1493del underlines the role of DIII-IV linker in Ca^{2+}-dependent regulation of coupled $Na_V1.5$ channels. The involvement of CaM and the details of Ca^{2+}-dependent regulation of $Na_V1.5$'s cooperative gating mechanism are yet to be determined.

$Na_V\beta1$ Regulates $Na_V1.5$ Gating Through CaM Interacting Domains

The interaction between monomeric $Na_V1.5$ during channel biogenesis is mediated by $Na_V\beta1$ (Mercier et al., 2012), but the involvement of $Na_V\beta1$ in the gating of coupled channels or in Ca^{2+}-dependent mechanisms have not been elucidated. The reported effects of $Na_V\beta1$ on $Na_V1.5$ gating parameters in mammalian expression systems are conflicting, generally suggesting that the cellular environment is critical for channel function (Calhoun and Isom, 2014). Similar to previous reports (An et al., 1998; Wingo et al., 2004; Zhu et al., 2017) we showed that $Na_V\beta1$ co-expression right-shifted $Na_V1.5_{WT}$ SSI curve (**Figure 4D**, bottom). Further, we showed that $Na_V\beta1$-induced a right-shift in $Na_V1.5_{WT}$ activation curve in the presence, but not in the absence, of Ca^{2+} (**Figure 4D**, top). This provides an indication for the role of Ca^{2+} in $Na_V\beta1$ regulation.

GFP-$Na_V1.5_{K1493del}$ altered $Na_V1.5_{WT}$ gating properties only when $Na_V\beta1$ was not expressed, whereas in the presence of $Na_V\beta1$, GFP-$Na_V1.5_{K1493del}$ expression did not affect gating. $Na_V\beta1$ was shown to modulate the voltage-sensor of $Na_V1.5$ domain IV (DIV, **Figure 1C**), and is believed to localize in close proximity to DIII-IV linker (Yan Z. et al., 2017; Zhu et al., 2017). Thus, we propose that $Na_V\beta1$ is intricately involved in the Ca^{2+}-dependent gating regulation, and can modify the contribution of DIII-IV linker to $Na_V1.5$ channels' cooperative-gating modulation.

Both effects of $Na_V\beta1$ on $Na_V1.5_{WT}$ were eliminated in $Na_V1.5_{A1924T*}$: the gating modulations and the loss of

$Na_V1.5_{K1493del}$ effect, indicating that A1924 residue may mediate $Na_V\beta1$ regulation. Interestingly, structural dimers were found in the CT of $Na_V1.5$. In the dimer, position 1924 is located in the interface of $Na_V1.5$ CT dimer, and A1924T mutation was shown to attenuate these interactions (Gabelli et al., 2014). In view of the structural and functional data, we suggest that cytosolic interaction between $Na_V\beta1$ and the IQ domain(s) in $Na_V1.5$ cytosolic CT, including A1924 residue, are involved in the regulation of $Na_V1.5$-gate. Since both DIII-IV linker and A1924T are thought to be included in the CaM-$Na_V1.5$ interaction complex, we postulate that $Na_V\beta1$ is part of a cytosolic CaM-interaction complex and a dynamic modulator of a complexed Ca^{2+}-regulated gate that comprises DIII-IV linker and the CT of multiple $Na_V1.5$ channels.

The Effect of $Na_V1.5$ Mutants on the Clinical Properties

Compound heterozygosity in *SCN5A* was associated with increased arrhythmic expression compared to heterozygotes in the same family. The clinical phenotype included severe bradycardia and conduction disease, which represents a reduction in electric activity of both the sinus-atria and the conduction system. Among the two mutations that were detected in the proband, the most striking biophysical feature is the loss-of-function due to K1493del mutation, which would lead to a 50% reduction in I_{Na} and haploinsufficiency. The changes in gating that arise from the second $Na_V1.5$ variant, A1924T*, are expected to have a relatively mild impact on cardiac rhythm but might have added to the pathological expression on the background of $Na_V1.5_{K1493del}$.

The physiological implication of Ca^{2+} modulation of $Na_V1.5$ is heart-rate dependent. During low-to-normal heart rate, I_{Na} transient of the cardiac action-potential precedes the Ca^{2+} transient and senses low Ca^{2+} levels. Repetitive and fast Ca^{2+} transients, during tachycardia, are expected to reveal Ca^{2+}-dependent conformational changes in protein complex formation that are limited by the association/dissociation rate, like $Na_V1.5$-CaM direct interaction, and other distal Ca^{2+}-induced pathways.

$Na_V1.5$ channels are physiologically modulated by $Na_V\beta1$ in cardiac cells (Edokobi and Isom, 2018). Interestingly, A1924T* mutant blunted $Na_V\beta1$- induced gating modulation. Close to resting potential and in the absence of Ca^{2+}, the availability of $Na_V1.5_{A1924T*}$ + $Na_V\beta1$ channels to open is two times lower than that of $Na_V1.5_{WT}$ + $Na_V\beta1$, which is expected to reduce the action-potential upstroke during low-to-normal heart rate (**Figure 4D**), and may explain the BrS phenotype reported in A1924T carriers (Rook et al., 1999). The addition of $Na_V1.5_{K1493del}$ on top of $Na_V1.5_{A1924T*}$ + $Na_V\beta1$ increased the number of $Na_V1.5$ channels available to open at rest (**Figure 4F**, right). This restoration of SSI properties may have moderated the development of BrS ECG pattern in the compound-heterozygote in our study, although a low penetration of A1924T phenotype cannot be ruled out.

In high Ca^{2+}, the window current of $Na_V1.5_{A1924T*}$ + $Na_V\beta1$ is shifted to hyperpolarized voltages comparing to $Na_V1.5_{WT}$, resulting in increased $Na_V1.5$ excitability. We speculate that this property can facilitate conduction and increase the propensity for development of exercise-induced atrial flutter with rapid ventricular response, on the background of bradycardia and conduction disease, that was demonstrated in the compound heterozygote in this study (**Figure 1A**, right).

It is noteworthy that certain loss-of-function mutations are expressed in BrS phenotype, e.g., A1924T, while others are associated with slow cardiac conduction and bradycardia, without BrS ECG pattern, e.g., K1493del [see also (Hu et al., 2010; Park et al., 2015)]. Possibly, the impaired mechanism that results in a loss-of-function plays a critical role in the downstream expression of the syndrome.

Extrapolation of the biophysical properties of mutated channels to disease expression, in the presented proband, is limited since we cannot determine the relative expression of each allele in the compound heterozygote cardiac cells, and thus we cannot determine the relative functional contribution of each mutated channel. In addition, the role of the polymorphism V1251M was not studied. The use of induced pluripotent stem-cells derived cardiomyocytes (iPSC-CMs), originated from the proband's cells, would be an attractive approach to investigate how the composite of mutations with distinct biophysical properties results in the cardiac phenotype, in a complex molecular environment, and in dynamic (Ca^{2+}) cycles.

CONCLUSION

We show that K1493del mutation induces a complete loss-of-function of $Na_V1.5$ due to gating, rather than biogenesis, defect. The effect of K1493 deletion is independent of the electric charge in this position. K1493del is associated with impaired CaM-interaction and Ca^{2+}-dependent modulation of sodium currents. $Na_V\beta1$ gating regulation is Ca^{2+}-dependent and involves the $Na_V1.5$ CT. These results highlight the role of $Na_V1.5$ DIII-IV linker in $Na_V1.5$-CaM-interaction and support a coupling between $Na_V1.5$ channels that is implicated in a Ca^{2+}-dependent gating mechanism.

ETHICS STATEMENT

The proband and his parents gave written informed consents for both the clinical and genetic studies, which were approved by the Institutional Ethics-Committee of the Sheba Medical Center, Tel-Hashomer (approval 2853/03).

AUTHOR CONTRIBUTIONS

SO and EN designed the research. SO planned the experiments, performed patch-clamp experiments, interpreted

the data, and wrote the manuscript. EN, RB, DL, and MG clinically evaluated the patient. MG acquired the financial support for the project. LV performed the biochemical experiments. EM prepared the DNA constructs, interpreted the data, and edited the manuscript. CA, JC, and EB performed and analyzed the genetic screen and edited the manuscript.

FUNDING

This work was supported by the Rothschild Caesarea Foundation and Dizengoff Trading Company (1952).

ACKNOWLEDGMENTS

The authors would like to thank Dr. Ronit S. Cherki for performing preliminary experiments. They also thank Ms. Elaine Finkelstein, Dr. Moshe Giladi, Dr. Moran Rubinstein, Dr. Sharon Weiss, Dr. Dahlia Palevski, and especially Prof. Nathan Dascal and Dr. Samuel Frere for reading the manuscript and for their helpful comments. The authors are grateful to Prof. T. Zimmer (Jena, Germany) for providing GFP-$Na_V1.5$ construct, Prof. L. Isom (Ann Arbor, MI, United States) for providing hβ1 construct, Prof. W.A. Catterall (Seattle, United States) for providing rβ1 construct and Prof. J. Adelman (Portland, United States) for providing CaM construct.

REFERENCES

Abdelsayed, M., Baruteau, A. E., Gibbs, K., Sanatani, S., Krahn, A. D., Probst, V., et al. (2017). Differential calcium sensitivity in NaV 1.5 mixed syndrome mutants. *J. Physiol.* 595, 6165–6186. doi: 10.1113/JP274536 doi: 10.1113/jp274536

Abriel, H. (2010). Cardiac sodium channel Na(v)1.5 and interacting proteins: physiology and pathophysiology. *J. Mol. Cell. Cardiol.* 48, 2–11. doi: 10.1016/j.yjmcc.2009.08.025

An, R. H., Wang, X. L., Kerem, B., Benhorin, J., Medina, A., Goldmit, M., et al. (1998). Novel LQT-3 mutation affects Na+ channel activity through interactions between alpha- and beta1-subunits. *Circ. Res.* 83, 141–146. doi: 10.1161/01.res.83.2.141

Armstrong, C. M., Bezanilla, F., and Rojas, E. (1973). Destruction of sodium conductance inactivation in squid axons perfused with pronase. *J. Gen. Physiol.* 62, 375–391. doi: 10.1085/jgp.62.4.375

Bechi, G., Rusconi, R., Cestele, S., Striano, P., Franceschetti, S., and Mantegazza, M. (2015). Rescuable folding defective NaV1.1 (SCN1A) mutants in epilepsy: properties, occurrence, and novel rescuing strategy with peptides targeted to the endoplasmic reticulum. *Neurobiol. Dis.* 75, 100–114. doi: 10.1016/j.nbd.2014.12.028

Ben-Johny, M., Yang, P. S., Niu, J., Yang, W., Joshi-Mukherjee, R., and Yue, D. T. (2014). Conservation of Ca2+/calmodulin regulation across Na and Ca2+ channels. *Cell* 157, 1657–1670. doi: 10.1016/j.cell.2014.04.035

Benson, D. W., Wang, D. W., Dyment, M., Knilans, T. K., Fish, F. A., Strieper, M. J., et al. (2003). Congenital sick sinus syndrome caused by recessive mutations in the cardiac sodium channel gene (SCN5A). *J. Clin. Invest.* 112, 1019–1028. doi: 10.1172/jci18062

Biswas, S., Disilvestre, D., Tian, Y., Halperin, V. L., and Tomaselli, G. F. (2009). Calcium-mediated dual-mode regulation of cardiac sodium channel gating. *Circ. Res.* 104, 870–878. doi: 10.1161/CIRCRESAHA.108.193565

Calhoun, J. D., and Isom, L. L. (2014). The role of non-pore-forming beta subunits in physiology and pathophysiology of voltage-gated sodium channels. *Handb. Exp. Pharmacol.* 221, 51–89. doi: 10.1007/978-3-642-41588-3_4

Cerrone, M., Lin, X., Zhang, M., Agullo-Pascual, E., Pfenniger, A., Chkourko Gusky, H., et al. (2014). Missense mutations in plakophilin-2 cause sodium current deficit and associate with a brugada syndrome phenotype. *Circulation* 129, 1092–1103. doi: 10.1161/CIRCULATIONAHA.113.003077

Chen-Izu, Y., Shaw, R. M., Pitt, G. S., Yarov-Yarovoy, V., Sack, J. T., Abriel, H., et al. (2015). Na+ channel function, regulation, structure, trafficking and sequestration. *J. Physiol.* 593, 1347–1360. doi: 10.1113/jphysiol.2014.281428

Chiang, D. Y., Kim, J. J., Valdes, S. O., De La Uz, C., Fan, Y., Orcutt, J., et al. (2015). Loss-of-function SCN5A mutations associated with sinus node dysfunction, atrial arrhythmias, and poor pacemaker capture. *Circ. Arrhythm. Electrophysiol.* 8, 1105–1112. doi: 10.1161/CIRCEP.115.003098

Clatot, J., Hoshi, M., Wan, X., Liu, H., Jain, A., Shinlapawittayatorn, K., et al. (2017). Voltage-gated sodium channels assemble and gate as dimers. *Nat. Commun.* 8:2077. doi: 10.1038/s41467-017-02262-0

Clatot, J., Zheng, Y., Girardeau, A., Liu, H., Laurita, K. R., Marionneau, C., et al. (2018). Mutant voltage-gated sodium channels can exert a dominant-negative effect through coupled gating. *Am. J. Physiol. Heart Circ. Physiol.* 315, H1250–H1257.

Clatot, J., Ziyadeh-Isleem, A., Maugenre, S., Denjoy, I., Liu, H., Dilanian, G., et al. (2012). Dominant-negative effect of SCN5A N-terminal mutations through the interaction of Na(v)1.5 alpha-subunits. *Cardiovasc. Res.* 96, 53–63. doi: 10.1093/cvr/cvs211

Claycomb, W. C., Lanson, N. A. Jr., Stallworth, B. S., Egeland, D. B., Delcarpio, J. B., Bahinski, A., et al. (1998). HL-1 cells: a cardiac muscle cell line that contracts and retains phenotypic characteristics of the adult cardiomyocyte. *Proc. Natl. Acad. Sci. U.S.A.* 95, 2979–2984. doi: 10.1073/pnas.95.6.2979

Deschenes, I., Neyroud, N., Disilvestre, D., Marban, E., Yue, D. T., and Tomaselli, G. F. (2002). Isoform-specific modulation of voltage-gated Na(+) channels by calmodulin. *Circ. Res.* 90, E49–E57.

Dixon, R. E., Moreno, C. M., Yuan, C., Opitz-Araya, X., Binder, M. D., Navedo, M. F., et al. (2015). Graded Ca(2)(+)/calmodulin-dependent coupling of voltage-gated CaV1.2 channels. *eLife* 4:e05608. doi: 10.7554/eLife.05608

Edokobi, N., and Isom, L. L. (2018). Voltage-gated sodium channel beta1/beta1b subunits regulate cardiac physiology and pathophysiology. *Front. Physiol.* 9:351. doi: 10.3389/fphys.2018.00351

Gabelli, S. B., Boto, A., Kuhns, V. H., Bianchet, M. A., Farinelli, F., Aripirala, S., et al. (2014). Regulation of the NaV1.5 cytoplasmic domain by calmodulin. *Nat. Commun.* 5:5126. doi: 10.1038/ncomms6126

Gabelli, S. B., Yoder, J. B., Tomaselli, G. F., and Amzel, L. M. (2016). Calmodulin and Ca(2+) control of voltage gated Na(+) channels. *Channels* 10, 45–54. doi: 10.1080/19336950.2015.1075677

Glynn, P., Musa, H., Wu, X., Unudurthi, S. D., Little, S., Qian, L., et al. (2015). Voltage-gated sodium channel phosphorylation at Ser571 regulates late current, arrhythmia, and cardiac function in vivo. *Circulation* 132, 567–577. doi: 10.1161/CIRCULATIONAHA.114.015218

Gui, J., Wang, T., Jones, R. P., Trump, D., Zimmer, T., and Lei, M. (2010). Multiple loss-of-function mechanisms contribute to SCN5A-related familial sick sinus syndrome. *PLoS One* 5:e10985. doi: 10.1371/journal.pone.0010985

Holst, A. G., Liang, B., Jespersen, T., Bundgaard, H., Haunso, S., Svendsen, J. H., et al. (2010). Sick sinus syndrome, progressive cardiac conduction disease, atrial flutter and ventricular tachycardia caused by a novel SCN5A mutation. *Cardiology* 115, 311–316. doi: 10.1159/000312747

Hoshi, M., Du, X. X., Shinlapawittayatorn, K., Liu, H., Chai, S., Wan, X., et al. (2014). Brugada syndrome disease phenotype explained in apparently benign sodium channel mutations. *Circ. Cardiovasc. Genet.* 7, 123–131. doi: 10.1161/CIRCGENETICS.113.000292

Hu, D., Barajas-Martinez, H., Nesterenko, V. V., Pfeiffer, R., Guerchicoff, A., Cordeiro, J. M., et al. (2010). Dual variation in SCN5A and CACNB2b underlies

the development of cardiac conduction disease without brugada syndrome. *Pacing Clin. Electrophysiol.* 33, 274–285. doi: 10.1111/j.1540-8159.2009.02642.x

Johnson, C. N. (2019). Calcium modulation of cardiac sodium channels. *J. Physiol.* [Epub ahead of print]

Johnson, C. N., Potet, F., Thompson, M. K., Kroncke, B. M., Glazer, A. M., Voehler, M. W., et al. (2018). A mechanism of calmodulin modulation of the human cardiac sodium channel. *Structure* 26:e683. doi: 10.1016/j.str.2018.03.005

Kapplinger, J. D., Giudicessi, J. R., Ye, D., Tester, D. J., Callis, T. E., Valdivia, C. R., et al. (2015). Enhanced classification of brugada syndrome-associated and long-QT syndrome-associated genetic variants in the SCN5A-encoded Na(v)1.5 cardiac sodium channel. *Circ. Cardiovasc. Genet.* 8, 582–595. doi: 10.1161/CIRCGENETICS.114.000831

Keller, D. I., Rougier, J. S., Kucera, J. P., Benammar, N., Fressart, V., Guicheney, P., et al. (2005). Brugada syndrome and fever: genetic and molecular characterization of patients carrying SCN5A mutations. *Cardiovasc. Res.* 67, 510–519. doi: 10.1016/j.cardiores.2005.03.024

Kim, J., Ghosh, S., Liu, H., Tateyama, M., Kass, R. S., and Pitt, G. S. (2004). Calmodulin mediates Ca2+ sensitivity of sodium channels. *J. Biol. Chem.* 279, 45004–45012. doi: 10.1074/jbc.m407286200

Kodama, I., Nikmaram, M. R., Boyett, M. R., Suzuki, R., Honjo, H., and Owen, J. M. (1997). Regional differences in the role of the Ca2+ and Na+ currents in pacemaker activity in the sinoatrial node. *Am. J. Physiol.* 272, H2793–H2806.

Lei, M., Huang, C. L., and Zhang, Y. (2008). Genetic Na+ channelopathies and sinus node dysfunction. *Prog. Biophys. Mol. Biol.* 98, 171–178. doi: 10.1016/j.pbiomolbio.2008.10.003

Li, Q., Huang, H., Liu, G., Lam, K., Rutberg, J., Green, M. S., et al. (2009). Gain-of-function mutation of Nav1.5 in atrial fibrillation enhances cellular excitability and lowers the threshold for action potential firing. *Biochem. Biophys. Res. Commun.* 380, 132–137. doi: 10.1016/j.bbrc.2009.01.052

Liu, M., Yang, K. C., and Dudley, S. C. Jr. (2016). Cardiac sodium channel mutations: why so many phenotypes? *Curr. Top. Membr.* 78, 513–559. doi: 10.1016/bs.ctm.2015.12.004

Lopez, K. N., Decker, J. A., Friedman, R. A., and Kim, J. J. (2011). Homozygous mutation in SCN5A associated with atrial quiescence, recalcitrant arrhythmias, and poor capture thresholds. *Heart Rhythm.* 8, 471–473. doi: 10.1016/j.hrthm.2010.10.014

Mercier, A., Clement, R., Harnois, T., Bourmeyster, N., Faivre, J. F., Findlay, I., et al. (2012). The beta1-subunit of Na(v)1.5 cardiac sodium channel is required for a dominant negative effect through alpha-alpha interaction. *PLoS One* 7:e48690. doi: 10.1371/journal.pone.0048690

Milanesi, R., Bucchi, A., and Baruscotti, M. (2015). The genetic basis for inherited forms of sinoatrial dysfunction and atrioventricular node dysfunction. *J. Interv. Card Electrophysiol.* 43, 121–134. doi: 10.1007/s10840-015-9998-z

O'malley, H. A., and Isom, L. L. (2015). Sodium channel beta subunits: emerging targets in channelopathies. *Annu. Rev. Physiol.* 77, 481–504. doi: 10.1146/annurev-physiol-021014-071846

Park, D. S., Cerrone, M., Morley, G., Vasquez, C., Fowler, S., Liu, N., et al. (2015). Genetically engineered SCN5A mutant pig hearts exhibit conduction defects and arrhythmias. *J. Clin. Invest.* 125, 403–412. doi: 10.1172/JCI76919

Pitt, G. S., and Lee, S. Y. (2016). Current view on regulation of voltage-gated sodium channels by calcium and auxiliary proteins. *Protein Sci.* 25, 1573–1584. doi: 10.1002/pro.2960

Poelzing, S., Forleo, C., Samodell, M., Dudash, L., Sorrentino, S., Anaclerio, M., et al. (2006). SCN5A polymorphism restores trafficking of a brugada syndrome mutation on a separate gene. *Circulation* 114, 368–376. doi: 10.1161/circulationaha.105.601294

Potet, F., Chagot, B., Anghelescu, M., Viswanathan, P. C., Stepanovic, S. Z., Kupershmidt, S., et al. (2009). Functional interactions between distinct sodium channel cytoplasmic domains through the action of calmodulin. *J. Biol. Chem.* 284, 8846–8854. doi: 10.1074/jbc.M806871200

Reinhard, K., Rougier, J. S., Ogrodnik, J., and Abriel, H. (2013). Electrophysiological properties of mouse and epitope-tagged human cardiac sodium channel Na v1.5 expressed in HEK293 cells. *F1000 Res.* 2:48. doi: 10.12688/f1000research.2-48.v2

Rook, M. B., Bezzina Alshinawi, C., Groenewegen, W. A., Van Gelder, I. C., Van Ginneken, A. C., Jongsma, H. J., et al. (1999). Human SCN5A gene mutations alter cardiac sodium channel kinetics and are associated with the brugada syndrome. *Cardiovasc. Res.* 44, 507–517. doi: 10.1016/s0008-6363(99)00350-8

Sarhan, M. F., Tung, C. C., Van Petegem, F., and Ahern, C. A. (2012). Crystallographic basis for calcium regulation of sodium channels. *Proc. Natl. Acad. Sci. U.S.A.* 109, 3558–3563. doi: 10.1073/pnas.1114748109

Sarhan, M. F., Van Petegem, F., and Ahern, C. A. (2009). A double tyrosine motif in the cardiac sodium channel domain III-IV linker couples calcium-dependent calmodulin binding to inactivation gating. *J. Biol. Chem.* 284, 33265–33274. doi: 10.1074/jbc.M109.052910

Schott, J. J., Alshinawi, C., Kyndt, F., Probst, V., Hoorntje, T. M., Hulsbeek, M., et al. (1999). Cardiac conduction defects associate with mutations in SCN5A. *Nat. Genet.* 23, 20–21. doi: 10.1038/12618

Shen, H., Zhou, Q., Pan, X., Li, Z., Wu, J., and Yan, N. (2017). Structure of a eukaryotic voltage-gated sodium channel at near-atomic resolution. *Science* 355:eaal4326. doi: 10.1126/science.aal4326

Sottas, V., and Abriel, H. (2016). Negative-dominance phenomenon with genetic variants of the cardiac sodium channel Nav1.5. *Biochim. Biophys. Acta* 1863, 1791–1798. doi: 10.1016/j.bbamcr.2016.02.013

Stühmer, W., Conti, F., Suzuki, H., Wang, X., Noda, M., Yahagi, N., et al. (1989). Structural parts involved in activation and inactivation of the sodium channel. *Nature* 339, 597–603. doi: 10.1038/339597a0

Tan, H. L., Bink-Boelkens, M. T., Bezzina, C. R., Viswanathan, P. C., Beaufort-Krol, G. C., Van Tintelen, P. J., et al. (2001). A sodium-channel mutation causes isolated cardiac conduction disease. *Nature* 409, 1043–1047. doi: 10.1038/35059090

Tan, H. L., Kupershmidt, S., Zhang, R., Stepanovic, S., Roden, D. M., Wilde, A. A., et al. (2002). A calcium sensor in the sodium channel modulates cardiac excitability. *Nature* 415, 442–447. doi: 10.1038/415442a

Van Petegem, F., Lobo, P. A., and Ahern, C. A. (2012). Seeing the forest through the trees: towards a unified view on physiological calcium regulation of voltage-gated sodium channels. *Biophys. J.* 103, 2243–2251. doi: 10.1016/j.bpj.2012.10.020

Verkerk, A. O., Amin, A. S., and Remme, C. A. (2018). Disease modifiers of inherited SCN5A channelopathy. *Front. Cardiovasc. Med.* 5:137. doi: 10.3389/fcvm.2018.00137

Wang, C., Chung, B. C., Yan, H., Wang, H. G., Lee, S. Y., and Pitt, G. S. (2014). Structural analyses of Ca(2)(+)/CaM interaction with NaV channel C-termini reveal mechanisms of calcium-dependent regulation. *Nat. Commun.* 5:4896. doi: 10.1038/ncomms5896

West, J. W., Patton, D. E., Scheuer, T., Wang, Y., Goldin, A. L., and Catterall, W. A. (1992). A cluster of hydrophobic amino acid residues required for fast Na(+)-channel inactivation. *Proc. Natl. Acad. Sci. U.S.A.* 89, 10910–10914. doi: 10.1073/pnas.89.22.10910

Wingo, T. L., Shah, V. N., Anderson, M. E., Lybrand, T. P., Chazin, W. J., and Balser, J. R. (2004). An EF-hand in the sodium channel couples intracellular calcium to cardiac excitability. *Nat. Struct. Mol. Biol.* 11, 219–225. doi: 10.1038/nsmb737

Yan, H., Wang, C., Marx, S. O., and Pitt, G. S. (2017). Calmodulin limits pathogenic Na+ channel persistent current. *J. Gen. Physiol.* 149, 277–293. doi: 10.1085/jgp.201611721

Yan, Z., Zhou, Q., Wang, L., Wu, J., Zhao, Y., Huang, G., et al. (2017). Structure of the Nav1.4-beta1 complex from electric Eel. *Cell* 170:e411. doi: 10.1016/j.cell.2017.06.039

Zhu, W., Voelker, T. L., Varga, Z., Schubert, A. R., Nerbonne, J. M., and Silva, J. R. (2017). Mechanisms of noncovalent beta subunit regulation of NaV channel gating. *J. Gen. Physiol.* [Epub ahead of print]

Zimmer, T., Biskup, C., Dugarmaa, S., Vogel, F., Steinbis, M., Bohle, T., et al. (2002). Functional expression of GFP-linked human heart sodium channel (hH1) and subcellular localization of the a subunit in HEK293 cells and dog cardiac myocytes. *J. Membr. Biol.* 186, 1–12. doi: 10.1007/s00232-001-0130-1

Ziyadeh-Isleem, A., Clatot, J., Duchatelet, S., Gandjbakhch, E., Denjoy, I., Hidden-Lucet, F., et al. (2014). A truncating SCN5A mutation combined with genetic variability causes sick sinus syndrome and early atrial fibrillation. *Heart Rhythm* 11, 1015–1023. doi: 10.1016/j.hrthm.2014.02.021

Zumhagen, S., Veldkamp, M. W., Stallmeyer, B., Baartscheer, A., Eckardt, L., Paul, M., et al. (2013). A heterozygous deletion mutation in the cardiac sodium channel gene SCN5A with loss- and gain-of-function characteristics manifests as isolated conduction disease, without signs of brugada or long QT syndrome. *PLoS One* 8:e67963. doi: 10.1371/journal.pone.0067963

Conflict of Interest Statement: The authors declare that the research was conducted in the absence of any commercial or financial relationships that could be construed as a potential conflict of interest.